ABSTRACT

LOVE, BRYAN MATTHEW. Mechanical and Laser Scribing For Use As Precision Shaping Techniques. (Under the direction of Jeffrey W. Eischen)

The purpose of this research has been to develop a model for mechanical and laser scribing processes used in the manufacture of hard disk drive heads. The scribing techniques are used to create small distortions on thin plates, allowing control over the shape of the plate. Analytical models for the scribing techniques allow more accurate control over the shape of the hard drive head, therefore increasing the performance of the drive. Using finite element techniques, prior models of mechanical scribing were extended to the three-dimensional case, allowing varying scribe length and placement. A force model for laser scribes was developed using similar finite element techniques and calibrated using experimental results. The laser scribing force model was parameterized, allowing the distortions by wide variety of scribes to be computed using simple equations. Consideration was given to modeling multiple scribes and complicated scribing geometries. Experimental results indicate that the model has a high degree of accuracy over a wide range of scribing geometries.

MECHANICAL AND LASER SCRIBING FOR USE AS PRECISION SHAPING TECHNIQUES

by

BRYAN MATTHEW LOVE

A thesis submitted to the Graduate Faculty of
North Carolina State University
in partial fulfillment of the
requirements for the Degree of
Master of Science

MECHANICAL ENGINEERING

Raleigh
2001

APPROVED BY:

R.O. Scattergood Thomas A Dow

W. E. C

Chair of Advisory Committee

To my parents, Tom and Karen Love.

Without your love and unending support,

none of this would have been possible.

Biography

Bryan Matthew Love was born on July 22nd, 1978 in Charlotte, North Carolina to Thomas and Karen Love. Bryan, along with his sister Amy, attended school in Charlotte for all thirteen years, graduating in 1996 from South Mecklenburg High School. In the following three years, Bryan completed his Bachelor of Science degree in Mechanical Engineering at North Carolina State University, graduating summa cum laude in the spring of 1999. Continuing study at North Carolina State, Bryan pursued his Master of Science degree in Mechanical Engineering, culminating in the defense of this thesis on May 8th, 2001. After graduation, Bryan will continue study at the Virginia Polytechnic Institute and State University, pursuing a doctorate in Engineering Science and Mechanics.

Acknowledgements

I could not have completed this thesis without the help and guidance of many people. Many thanks to:

- Dr. Jeffrey Eischen, for guiding me through this project, offering tips and suggestions when needed, and helping me catch my multitude of mistakes.
- Dr. Thomas Dow and the rest of the Precision Engineering Center, for broadening my education and experience and making me consider things that are often overlooked.
- Dr. Ronald Scattergood, for the intuitive insights on the nature of mechanical and laser scribing that led to some of the breakthroughs in my work.
- Donnie Moorefield and Hee Park of IBM, for practical information on laser scribing and their assistance with the experimental work performed at IBM.
- and most of all, my friends and family, for supporting me, encouraging me, and reminding me that life can be truly wonderful.

Table of Contents

List of Figures

List of Tables

1 Introduction

1.1 Background and Objective of Research

As the world becomes increasingly more dependent on computers, the speed and reliability of electronic storage (e.g. hard disk drives) has become a critical issue. Data density and hard drive speed are doubling approximately every eleven months. This rapid rate of increase demands constant refinement of materials processing and manufacturing techniques. A primary influence on the data density and speed of a hard drive is the flying height of the read/write electronics (*head* in the hard drive industry). The read/write heads are contained on a small ceramic *slider* that acts as an air bearing when the disk is in motion. Figure 1.1 shows a photograph of a typical hard disk drive.

Figure 1.1. Modern Hard Disk Drive

As the storage disk rotates, it creates a boundary layer that causes the ceramic slider to "fly" over the surface. The shape of the slider determines how much lift or downforce is

generated and, therefore, the flying height of the read/write head. The slider flying height in modern hard drive is on the order of twenty-five nanometers and is decreasing rapidly due to industry demands (Tam, et. al. (1999)). Therefore, accurate control over the shape of the slider on the nanometer level is paramount to future performance and reliability improvements.

Scribing is one technique where the ability for nanometer-level shape control has been demonstrated. An older technique is mechanical scribing, which utilizes a diamond indenter to scratch the surface of the slider, thus producing some residual stress and the corresponding deflection. This technique has been studied extensively by Austin and Scattergood, but only in limited geometries (Austin (2000)). A newer technique utilizes a laser to induce localized stress on the slider—this technique brings the advantages of using optics for precise control and speed (millions of sliders are produced a day). Both of these techniques have been in use for quite some time now. For successful application, each technique requires trial-and-error experimental history or closed loop feedback to control the shape generated by the scribing. Thus, the objective of the present research is to develop a computational model that can accurately predict the deflections generated by scribes (both mechanical and laser) and to apply this model to previously untested scribing geometries. With an accurate model, a system could be developed where a desired shape could be produced using a predicted scribing pattern.

1.2 Modeling Techniques

Predicting the generation of residual stress due to scribing is difficult because it involves plastic deformation (mechanical) and/or phase change (laser). However, a force system can be calibrated to closely mimic the residual stresses induced by the scribing; such techniques have been carried out by Yoffe (1982) and, more recently, Austin (Austin (2000)). These techniques utilize a force system on a theoretical model to produce a deflected shape. This deflected shape is then "calibrated" to a single experimental result and can be used to solve for other scribing geometries and loads. However, past techniques have relied on simple geometries and assumptions to aid in calculation—the solution of a scribe of any length on any part of the slider is not theoretically feasible. However, numerical techniques such as finite elements allow more complicated geometries to be modeled accurately. A similar technique can be used: a force system can be applied to a finite element mesh and then calibrated to an experimental result. The resulting model can then be used to predict other scribe results for different lengths, placements, and directions. Furthermore, a linear finite element analysis allows single scribe results to be superposed to give the results for multiple scribes. Thus, a library of single scribe solutions can be used to predict the most complicated of scribing patterns. Preliminary research demonstrates how a library of such results could be used to find a particular pattern to produce a desired shape.

1.3 Literature Review

There is little documentation of theoretical or experimental studies of scribing processes. Yoffe (1982) developed a twin-dipole model for indenting brittle materials—the technique utilizes a pair of experimentally calibrated dipoles on an elastic half space to model the stress field produced by indentation of a brittle material with a Vickers type indenter. Ahn, et. al. (1993) extended the indentation model to the scribing case by integrating Yoffe's result. The integration produces the solution for a line dipole on an elastic half space—representing a mechanical scribe. Scattergood utilized Ahn's solution to find the deflections produced by a mechanical scribe on a finite thickness plate by applying principles of superposition and a beam theory approximation. Further research at North Carolina State University conduced by Austin (2000), calibrated and verified Scattergood's model using a particular ceramic material used in the construction of hard disk drive heads. The calibrated line dipole model (Scattergood-Austin) shows excellent correlation with experimental results. The previous research has shown that the line dipole model can successfully predict the deflections produced by mechanical scribing. The present research seeks to extend this model to scribing geometries and multiple scribe patterns not possible with the simplistic models used in the past.

Laser scribing is a new technique with little literature on past research. Most of the published research focuses on techniques that rely on laser ablation (the removal of material), annealing, and the use of lasers for crystallographic modification. Liu (1999) documents the effects of lasers and the deformations produced on hard disk surfaces, but the research focuses on the local texturing and is purely empirical. Liu however does indicate that the melt/solidification process produces localized stress and deformation.

The sole public domain source of information on laser scribing is from IBM's Almaden Research Center, published in December of 1999 (Tam, et. al.). IBM pioneered the technique of shaping ceramic plates through the use of a controlled pulsed laser, but no modeling of the process was conducted. The current research allows the laser scribing process to be modeled, and the deflections caused by a scribing pattern to be predicted for a wide range of scribing geometries.

2 Mechanical Scribing

2.1 Theoretical Model

Mechanical scribing is the older (and more well documented) of the two scribing techniques. A mechanical scribe is produced by dragging the corner of a cubic indenter against the surface of a slider. This technique causes plastic deformation of the material and a localized area of compressive residual stress (see Figure 2.1a), along with a minute deflection of the slider *away* from the scribed side (see Figure 2.1b).

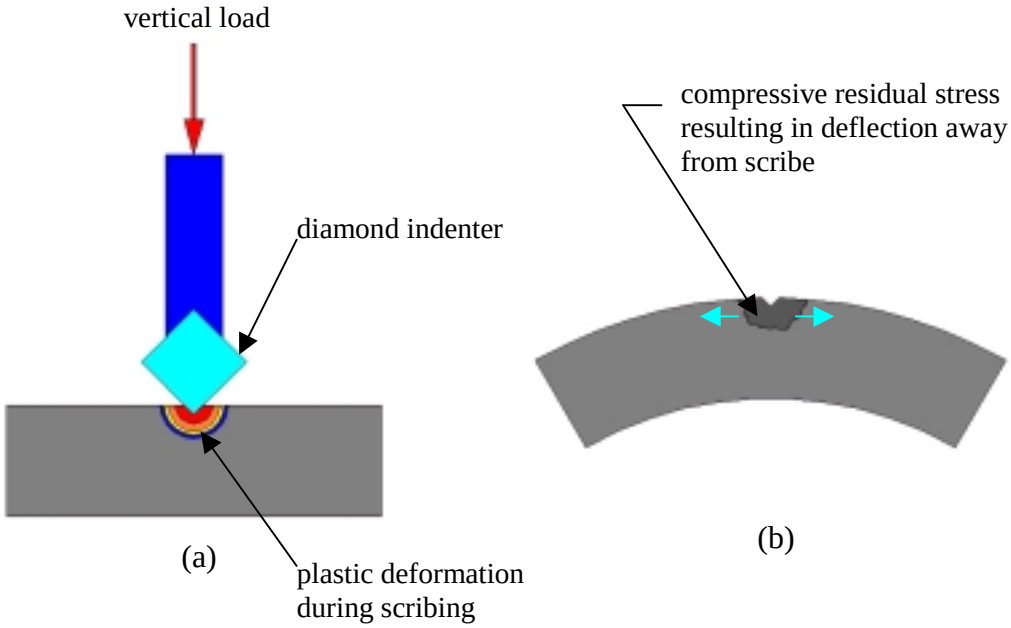

Figure 2.1. Mechanical Scribing Process

The determination of the residual stress field and predicting the deflections for the mechanical scribe is difficult; however, several models have been developed to predict deflections and stresses due to indentations and scribes. Yoffe (1982) used a pair of

orthogonal force dipoles to model the residual stresses created by indentation on an elastic half-space. A previously developed model for mechanical scribing views the scribe as the superposition of a line of these dipoles (Ahn, et. al. (1993)). The forces in the scribing direction cancel during superposition (the end forces were neglected in Ahn's model), resulting in the line dipole shown in Figure 2.2. This model has an exact

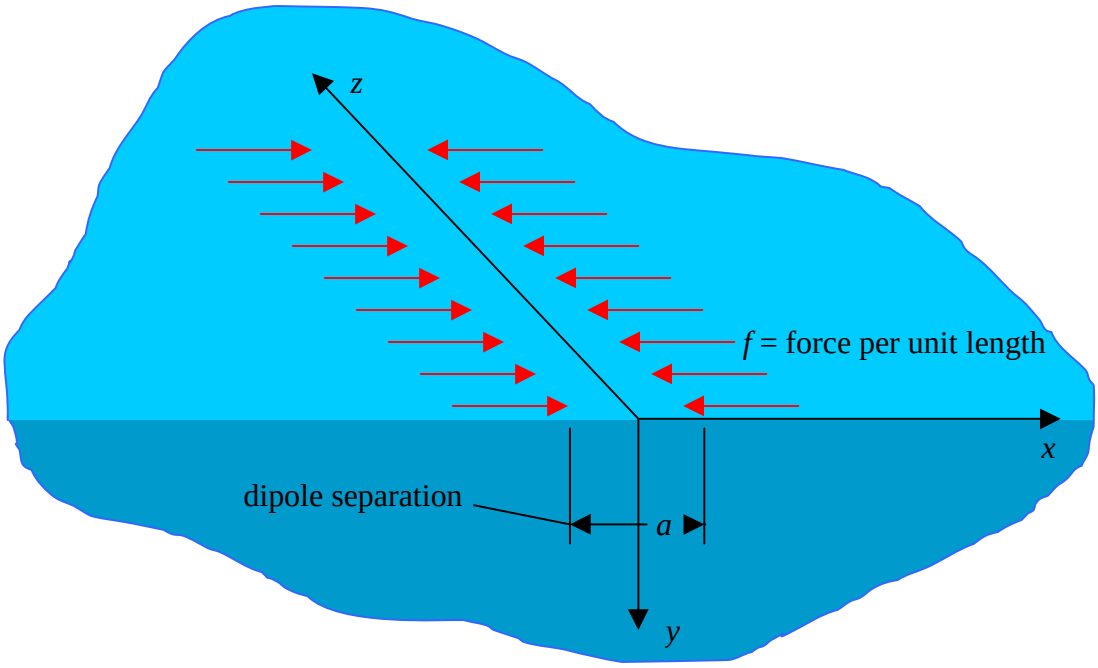

Figure 2.2. Line Dipole on Elastic Half Space As a Model for Mechanical Scribing

theoretical solution for both stress and deflection, but it requires that the associated structure be semi-infinite. Scattergood (2000) utilized this solution to develop a simple two-dimensional model designed to approximate the solution for a plate with finite dimensions (valid for the plane stress/strain case). The finite plate is cut out of the semi-infinite solid, and the reverse tractions are applied to the bottom and edge surfaces of the plate. Beam theory is then implemented to solve for the deflection created by the reverse tractions and the deflections are superposed with the deflections created by the line

dipole. The result is an approximate solution for the finite plate with a line dipole. Figure 2.3 shows the resulting deflection and Scattergood's solution.

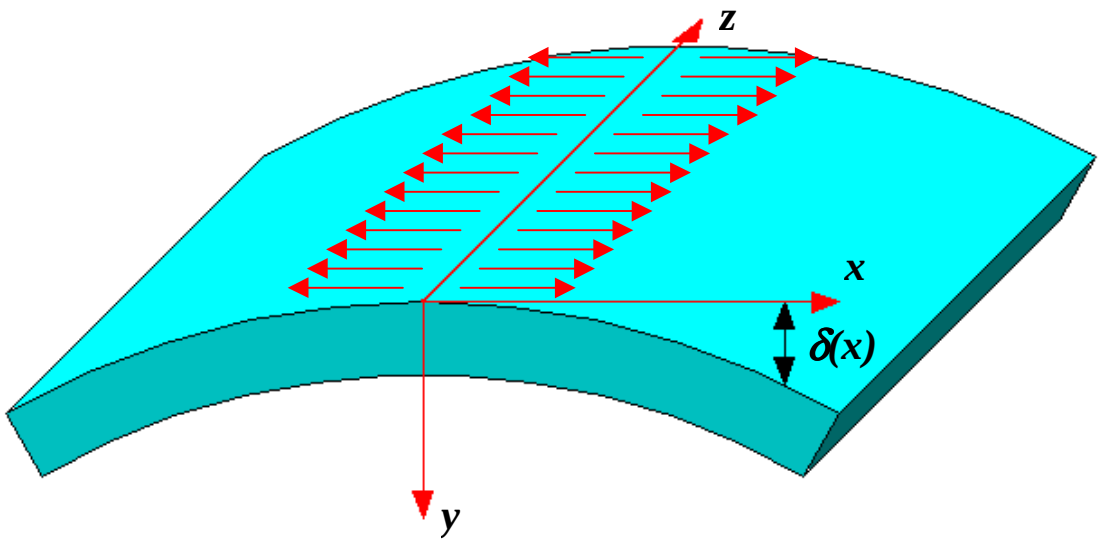

$$\delta(x) = -\frac{6B}{\pi E h}\left[\frac{x}{h}\tan^{-1}\left(\frac{x}{h}\right)\right] \qquad (1)$$

Figure 2.3. Deflection of Finite Plate Mechanical Scribing Model

Scattergood's equation (equation 1) gives the deflection in terms of B (the dipole strength, B is the product of the force per unit length f and the dipole separation a), the thickness of the plate h, the elastic modulus E, and the position x. However, this equation cannot directly give the deflection. The model requires calibration since the magnitude of the line dipole is generally unknown. Austin (2000) approached this calibration directly by performing experiments with varying the vertical load on the scribing tool W (see Figure 2.1). Experiments were conducted using a material composed of alumina and titanium carbide (AlTiC). This material is currently used in read/write slider applications.

Comparing the deflections generated by the model and the actual experiments, Austin developed a calibration equation that expresses B in terms of W for AlTiC:

$$B = 0.0332 + 0.516W + 0.291W^2$$

Using this empirically derived relation, Scattergood's model can be used to predict the deflection of a mechanical scribe to within a few percent.

2.2 Finite Element Modeling for Mechanical Scribes

Several assumptions were made in the derivation of Scattergood's theoretical solution. The actual elasticity solution to predict the deflection of a truly finite plate is unwieldy and impractical (and it possibly has no closed form solution), therefore numerical techniques are sought.

Finite element analysis is a well-documented numerical technique with many robust commercially available software packages. It allows the solution of three-dimensional elasticity problems through the discretization of the solid using connected elements. These elements have limited capability (in terms of the deflections they allow), but the finite element solution approaches the elasticity solution as the number of elements is increased (particularly in areas of high strain). The scribing finite element models are linear elastic models—deflections and stresses are directly proportional to the loading (twice as much force generates twice as much deflection) and inversely proportional to material stiffness (if E is scaled up by a factor of three, deflections are one-third of the original values). More detail on finite element meshing techniques, restraints, and loading conditions is given in Section 4.1.

Mechanical scribing has a very localized effect—both Austin's experiments and Scattergood's model show that the scribe has very little influence on deflection beyond two to three scribe widths, and the stress fields shown by Yoffe (1982) and Ahn (1993) are also on this scale. Therefore, the finite element mesh must model this localized stress region—requiring a fine mesh around the scribe. However, after a small distance, the stress levels are negligible and the element size can be increased to speed up computational time without any impact on accuracy.

Considering the requirements for the scribing problem, a finite element mesh was developed in ANSYS 5.6 (a widely recognized and commercially available finite element package). The finite element mesh shown in Figure 2.4. utilizes quarter-symmetry

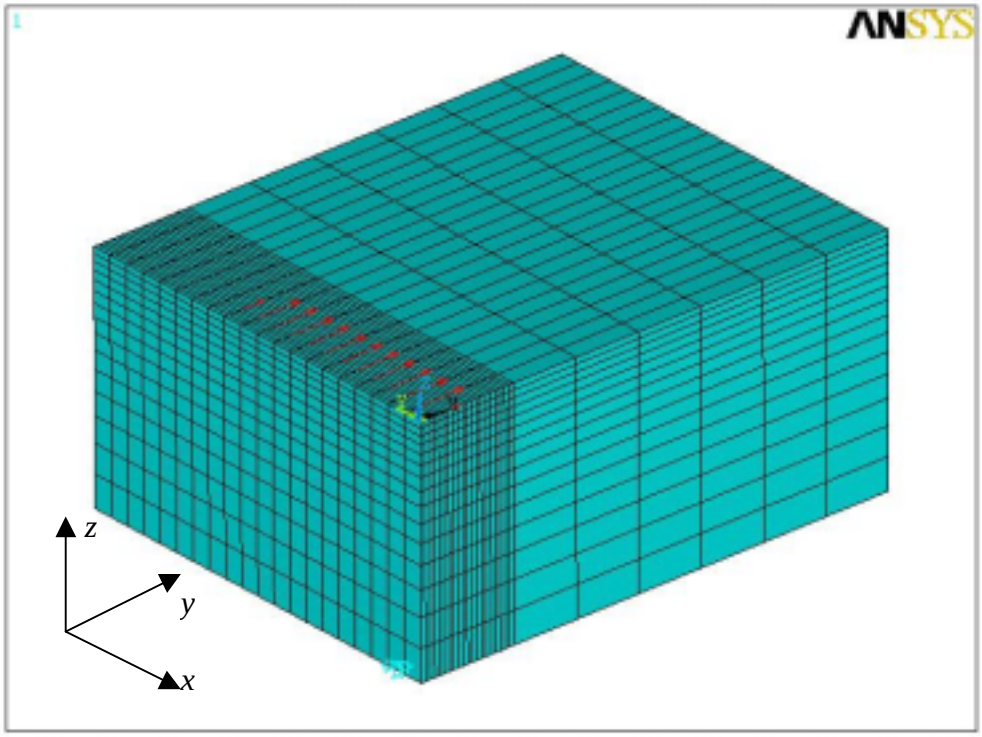

Figure 2.4. Finite Element Mesh for Mechanical Scribing Simulations

(symmetry planes on the faces on the left and right) to model a centrally located scribe.

The quarter-symmetry slider model measures 0.625 mm by 0.5 mm by 0.3 mm, while the actual slider is 1.25 mm by 1.0 mm by 0.3 mm. To capture the stress field created by the line dipole scribe, a densely meshed region was created in the *y* direction around the scribe location. Figure 2.5 shows the stress field due to an applied scribe—note the localized effect of the scribe.

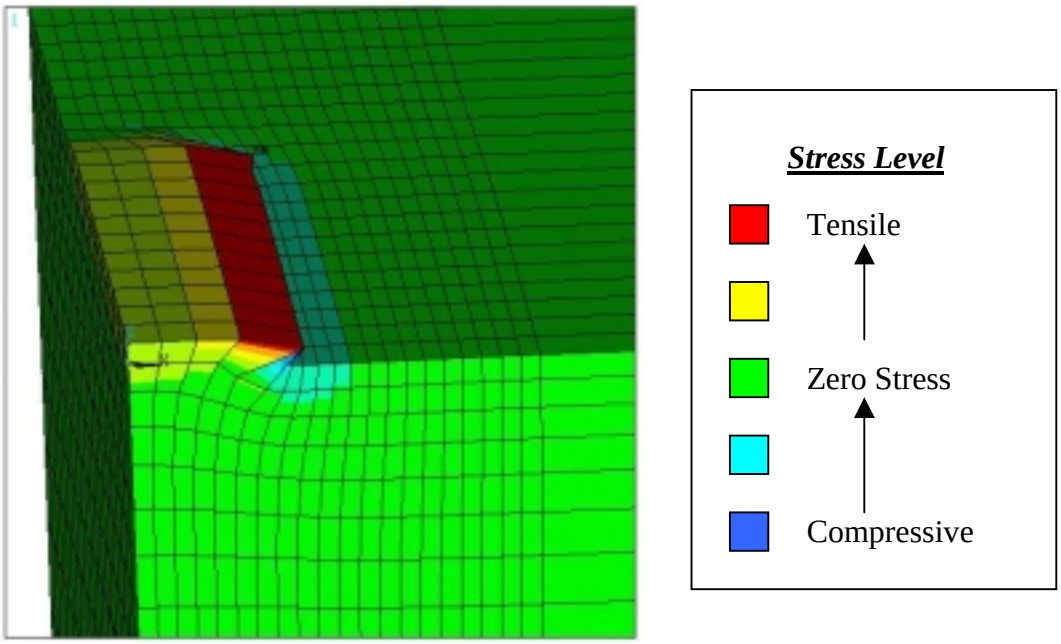

Figure 2.5. Localized Stress Due to Mechanical Scribe

To model the scribe, a line force of magnitude 10.25 N/mm was applied all the way across the 0.5 mm direction (to mimic a complete scribe on a slider—an experiment previously performed by Austin and calibrated by Scattergood). The scribe separation was set at 8 elements (or 4 to the symmetry line), representing a dipole separation of 0.04167 mm. Using ANSYS 5.6, the solution was found for this model and is shown in Figure 2.6. Note that the large spike in the data is an artifact of the finite element model and should not be considered when comparing the finite element model to actual

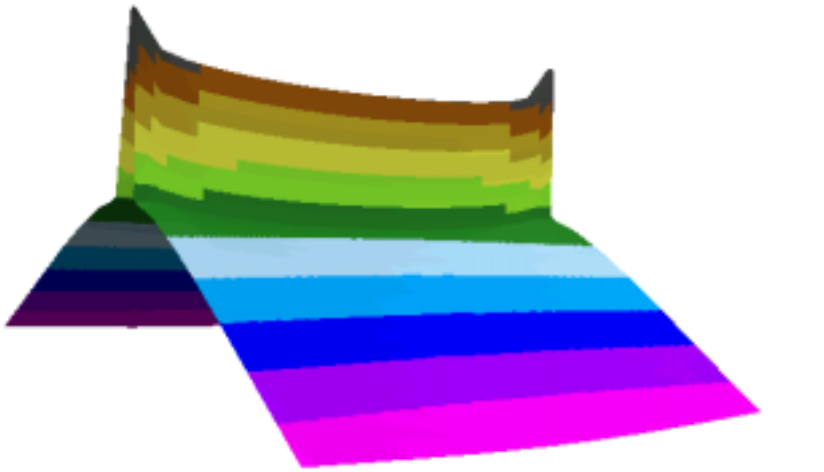

Figure 2.6. Mechanical Scribe Model Result
For Full Scribe in *x* Direction

deflections seen in experiments. One interesting aspect of the model is the small amount of curvature present in the direction parallel to the scribe. This curvature is often termed "anticlastic" curvature, and is an effect generated by Poisson's ratio. The anticlastic curvature is small and in the opposite direction as the primary deflection. Assumptions made in Scattergood's model do not allow the anticlastic curvature to arise in the solution.

Further comparison between the finite element model and the beam theory model show that they agree within a few percent. Figure 2.7 shows a plot of the deflections predicted by the two models when B = 5 N/mm, E = 1 N/mm^2, and h = 0.3 mm. Again, note that the spike in the center of the data in the finite element curve is an artifact of the analysis and would not be present in actual data. The tip deflections of the two models differ by 8.7%, and the general shape of the two data sets is similar. The difference in the tip deflection is due to Scattergood's use of beam theory in his model—beam theory does not account for shear traction effects that are present in the finite element model.

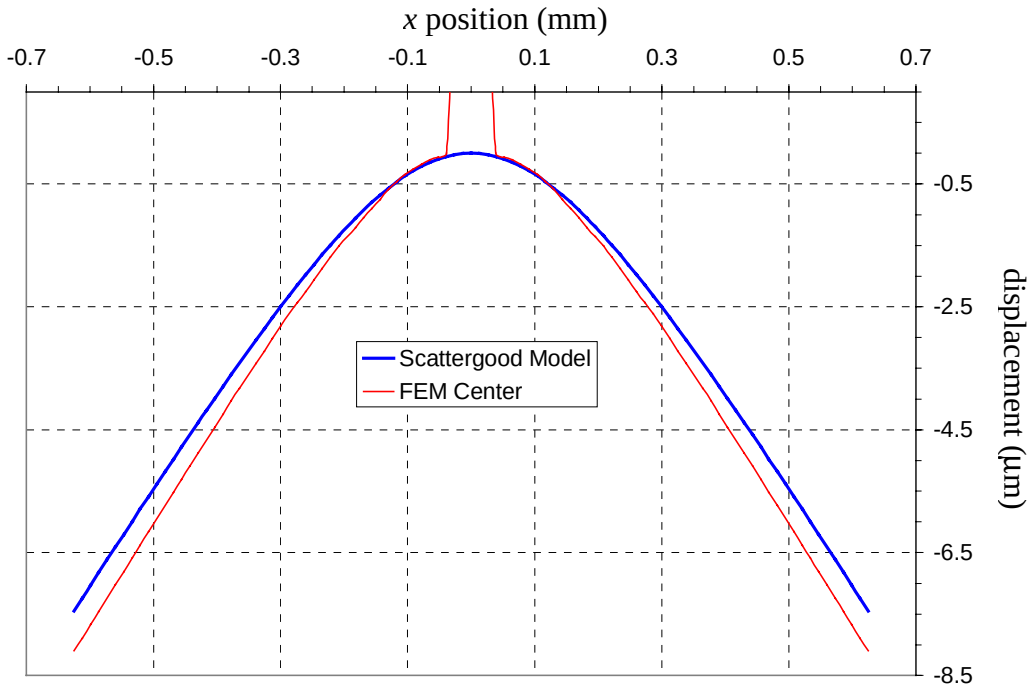

Figure 2.7. Comparison of Scattergood Beam Theory Model with Finite Element Analysis

Since the finite element analysis is inherently linear (as is the beam theory model), the calibration curve can simply be scaled and a similarly accurate calibration curve obtained. With an accurate calibration curve, the finite element technique can be used for varying scribe widths, as well as changing the orientation and placement.

2.3 Extension of Scribing Model Using Finite Elements

Mechanical scribing has been employed to control the shape of sliders for several years. However, to reach the levels of shape control necessary in the construction of a

new generation of sliders, better understanding of the deflections caused by mechanical scribes is needed. The Scattergood model (calibrated by Austin) allows accurate prediction of the deflection generated by mechanical scribes that extend across the full width of the slider. However, it does not allow scribes with a finite length or asymmetrically place scribes. It has been demonstrated that a calibrated finite element model can accurately model the scribing process. Also, the finite element model allows solutions for more complicated scribing geometries.

To determine the effect of scribe length, the finite element model was used to simulate mechanical scribes with varying lengths centered on the slider, oriented parallel to the edges. The model varied scribe lengths from 200 μm to 1000 μm (full width scribe). Figure 2.8 below shows the shape of the slider as a function of scribe length (200 and 300 μm scribes were eliminated from the plot for clarity). Note the anticlastic

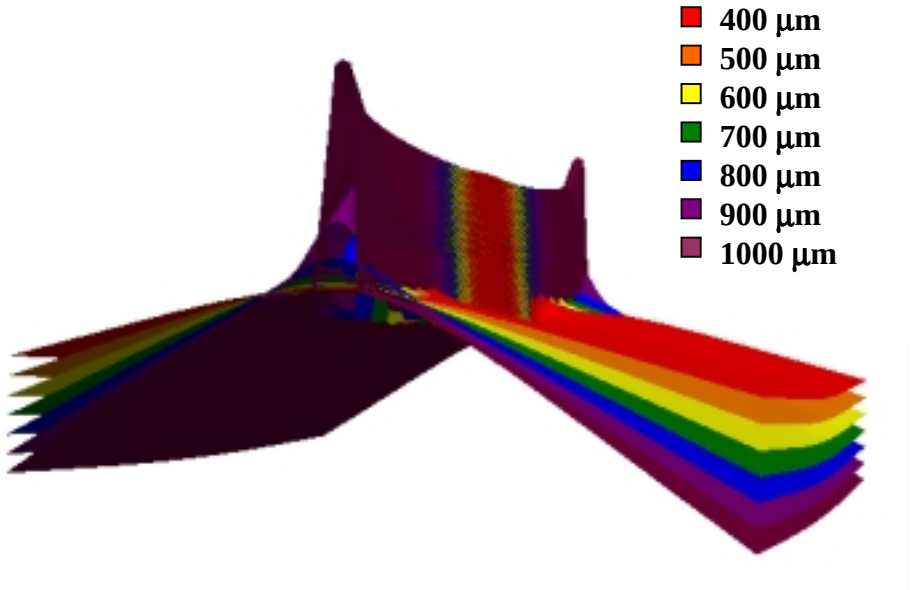

Figure 2.8. Deflections Generated by Partial Length Mechanical Scribes

curvature in each case. Figure 2.9 shows both the primary and anticlastic curvatures as a

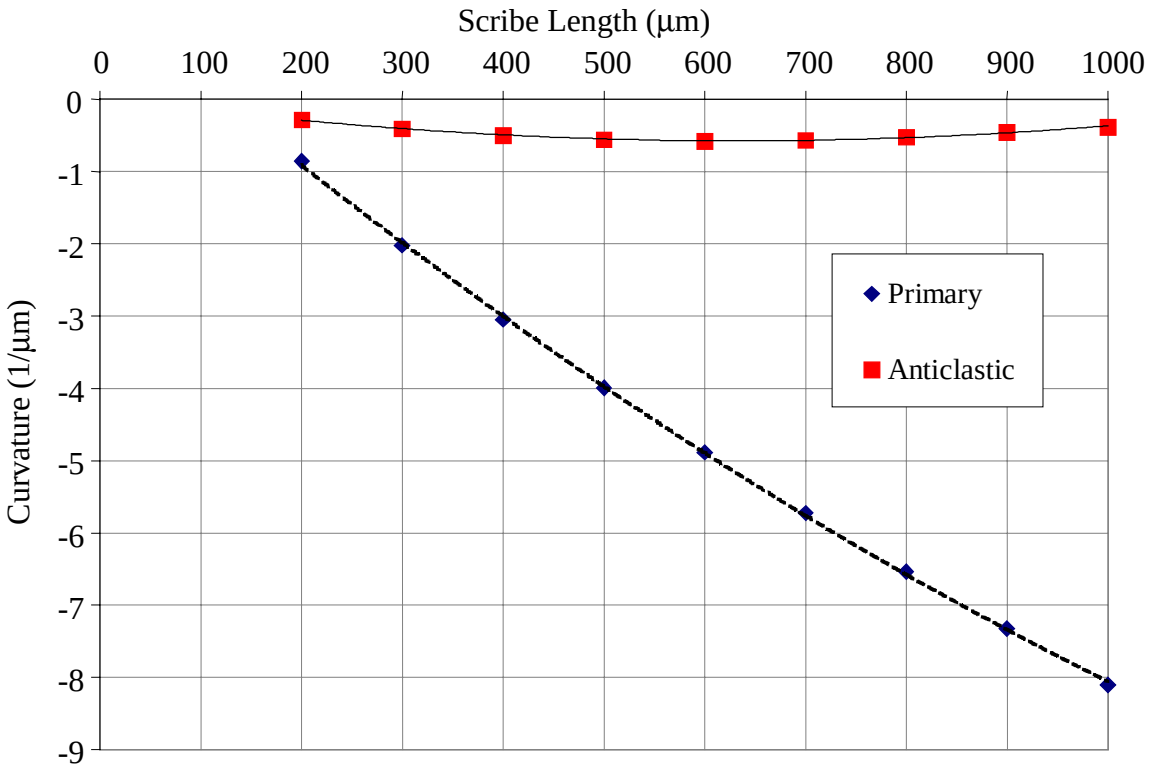

Figure 2.9. Primary and Anticlastic Curvatures as a Function of Scribe Length

function of scribe length. Plotting trendlines (shown in Figure 2.9) through the data shows that both curvatures have a parabolic dependence on scribe length (R^2 values are greater than 0.995). Using this parabolic dependence, the correct scribe length to obtain a desired deflection can be calculated—allowing precise control of the shape of the slider without intermediate measurement or closed loop control.

The use of finite elements also allows solution of other scribing geometries that would be very difficult through analytical techniques. Figure 2.10 shows the deflection generated by a scribe offset from the centerline of the slider. Scribing is frequently used as a curvature correction technique, and correcting for deflection not removed from the sliders by lapping could possibly require off-axis or even diagonal scribes. The finite element approach allows the deflection generated by these scribes to be predicted and,

through the use of superposition and a library of results, a scribing pattern to produce the desired deflection can be found.

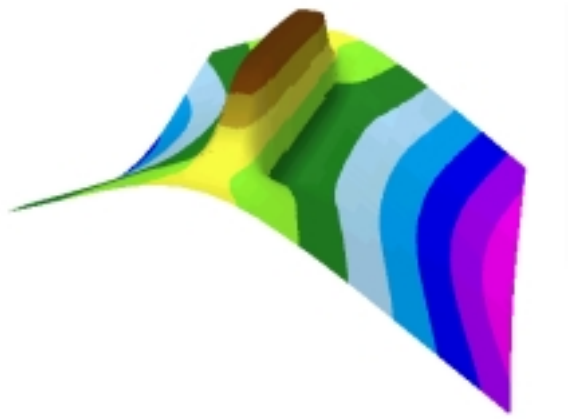

Figure 2.10. Deflection Generated by Asymmetrical Scribe Placement

In the past few years, new techniques have replaced mechanical scribing as a curvature adjustment technique. In production, mechanical scribing is time consuming and produces deflections on the order of 10 to 100 nm with reasonable precision. A new technique pioneered by IBM uses a laser to produce curvature on the sliders—it has the benefits of being much faster than mechanical scribing and produces deflections on the order of 1 nm with a high degree of precision. As with mechanical scribing, a model to predict the deflections produced by laser scribing is needed as the demands on data density and hard drive speed increase.

3 Laser Scribing

3.1 Background and Theoretical Approach

Laser scribing is a newer technique for controlling the shape of sliders. IBM, one of the major manufacturers of read/write heads in the United States, pioneered this field and created a system known as the Laser Curvature Adjust Technique (LCAT) (Tam (1999)). Figure 3.1 illustrates the simple technique: a pulsed laser is focused on the surface of the ceramic slider, and with sufficient power input a small circle of material is melted. The solidification of this material results in a localized stress around the circle—the ceramic shrinks as it solidifies and the material outside the dot is placed in tension. If a line of dots is created, the spacing between the dots can be decreased until it resembles a solid line. Studies at IBM have shown that as the dot spacing is decreased, the resulting deflection saturates, producing a continuous, repeatable "scribe" (Tam, et. al. (1999)). The laser can be accurately controlled by a set of galvo mirrors, thus allowing the LCAT

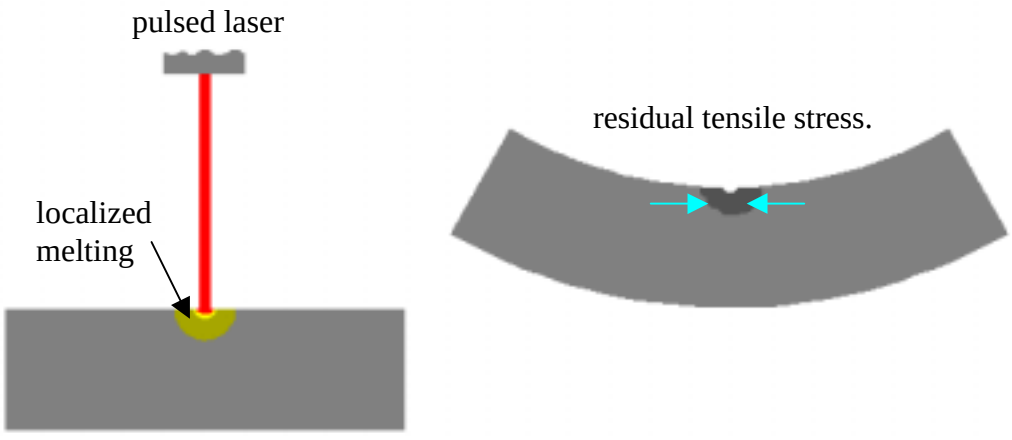

Figure 3.1. Laser Scribing Process

system to place scribes of varying lengths anywhere on the surface of the slider.

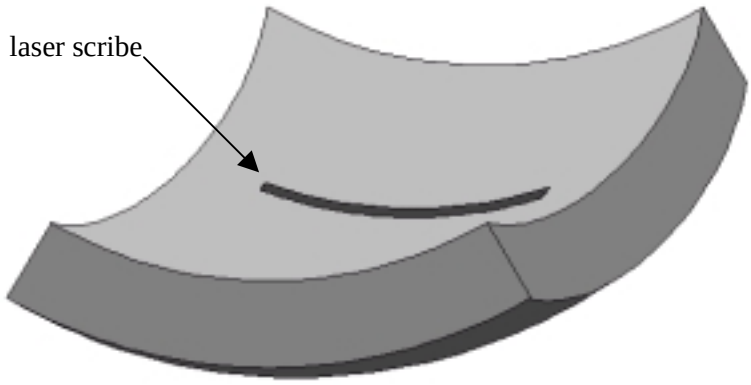

Figure 3.2. Illustration of Laser Scribed Slider

The stresses and deflections created by laser scribing differ from mechanical scribing in several ways. The most obvious is that laser scribes produce residual tension, rather than the compression, resulting in the slider bending towards the scribe as show in Figure 3.1. Secondly, laser scribes produce appreciable curvature in the *both* directions relative to the scribe axis. These curvatures are of the same order of magnitude and in the same direction (shown in Figure 3.2). Compare this response with the very small, opposite-direction anticlastic curvature generated by mechanical scribing.

While the two types of scribing generate different deflections, they both induce localized areas of stress. The line dipole force system that accurately modeled mechanical scribing can be extended to the laser scribing case with some modification. The direction of the forces needs to be changed; the curvature generated by laser scribing is in the reverse of the curvature generated by mechanical scribing. The line dipole, however, does not produce the curvature in the parallel direction as seen in laser scribing.

An extension to the model must be made to compensate for this effect. Figure 3.3 shows two proposals for force systems to model laser scribing. In both models, the familiar line dipole forces f_M (force per unit length) produce curvature perpendicular to the scribe. The parallel curvature is generated by the application of a uniform force f_m (force per unit length) in the line force model, while the end force model relies on forces F_m to produce the parallel curvature. Just as with the mechanical scribing, these models must be calibrated with experimental results.

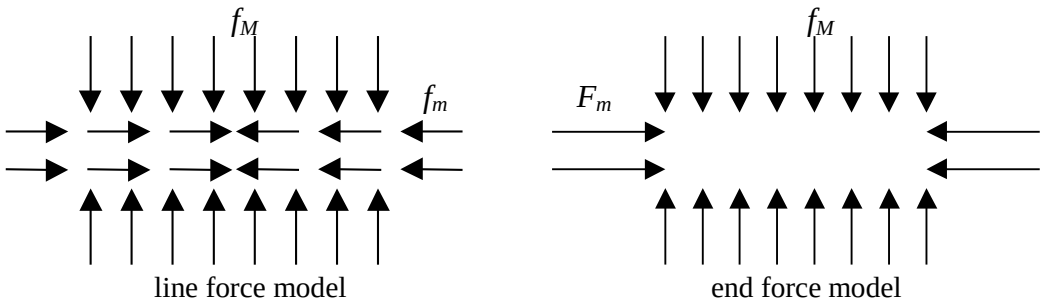

Figure 3.3. Laser Scribing Force Models

3.2 Nomenclature

The read/write head industry has developed its own terminology to describe the size and shape of sliders. The particular terms and conventions presented here are those used by IBM. The sliders are constructed of an alumina-titanium carbide (AlTiC) ceramic, and are approximately 1.25 mm by 1.07 mm by 0.30 mm (this size is know as the “pico” slider). Forty-four sliders are attached along the 1.25mm edge, resulting in a 47mm by 1.25mm by 0.3mm *row* (shown in Figure 3.4). The two large surfaces are known as the air bearing surface (ABS side) and the flex side. The ABS side flies over the surface of

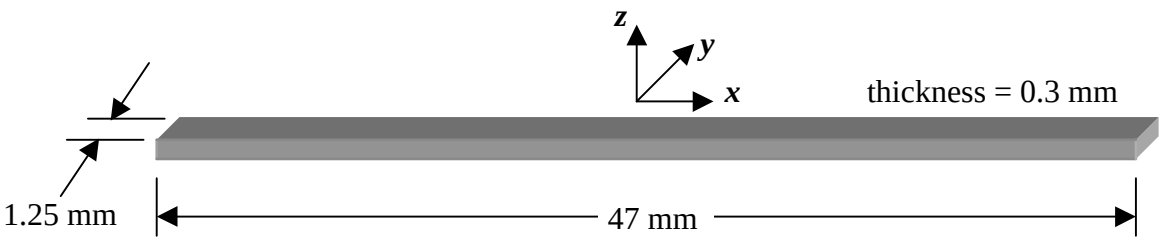

Figure 3.4. Row of Sliders

the storage disk, while all scribing is performed on the flex side. The shape of the ABS side determines the flying height, so each slider's ABS side is measured while the flex side is scribed. The out of plane deflection *w*, of the ABS side is fitted with a biquadratic curve as follows:

$$w = f(x,y) = C_0 + C_1x + C_2y + C_3x^2 + C_4y^2 + C_5xy \qquad (2)$$

where *x* and *y* and *z* are defined in Figure 3.4. The first three coefficients describe the best-fit plane through the surface (thus removing any rigid body rotations from the data). The final three coefficients define curvatures that are important in the aerodynamics that determine the flying height. These curvatures are normalized and defined as crown, camber, and twist:

$$\textbf{Crown} = -C_4L^2/4 \qquad (3)$$

$$\textbf{Camber} = -C_3W^2/4 \qquad (4)$$

$$\textbf{Twist} = -C_5LW \qquad (5)$$

where *L* and *W* are the length and width of the ABS side (*L* = *W* = 1mm for IBM's purposes). The negative signs define positive curvature as curvature that lift the corners away from the storage disk. Figure 3.5 shows a graphical representation of crown, camber, twist, and the coordinate system. Note that in this diagram, crown is positive and camber is negative.

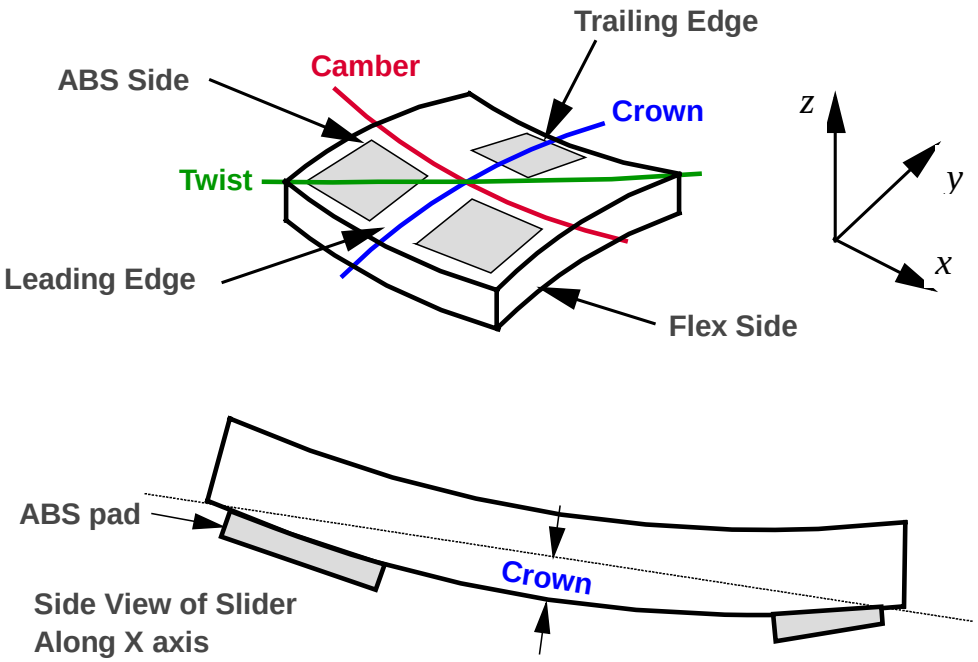

Figure 3.5. Slider Coordinate System and Curvature Definitions

Crown is the primary influence on slider flying height, but control over camber and twist is essential for performance improvement. Currently, crown can be controlled accurately with the LCAT system—usually, to the nearest nanometer. Due to current capabilities and demands, the amount of camber created by the scribing pattern is directly proportional to the amount of crown and there is very little compensation for twist. The asymmetry represented by twist is a major problem in slider construction; in fact, one of the major objectives of this project is to develop scribing patterns to remove twist from a slider.

3.3 Experimental Metrology

Measuring and handling of parts on this scale can be challenging and requires special considerations. To provide an accurate representation of industrial techniques and practices, all tests were conducted at IBM-San Jose, utilizing their laser scribing (LCAT) and metrology equipment. As stated previously, sliders are measured and scribed while still part of a row—making handling much simpler and requiring less complicated fixtures and shorter set up times. Currently, sliders are scribed and measured in a closed-loop system, described in more detail by Tam (Tam, et. al. (1999)). The LCAT accepts fixtures that hold 24 rows (a total of 1056 sliders) utilizing a vacuum system. An *x-y* positioning stage permits any slider to be viewed (from both sides) and scribed on the flex side. Once the sliders are loaded in the LCAT, each is scribed several times and curvatures are measured using an internal optical measuring device. The process is repeated until the sliders reach a desired shape. The effect of a single scribe is not directly observed in the process; the final shape of the ABS side is the only consideration. Therefore, to accurately study the effects of scribes, a different technique is needed.

To measure the effects of laser scribes on sliders, an accurate determination of the shape of the slider before and after scribing is necessary. A laser (phase shift) interferometer (specifically, a Wyko HD-2000) was used to determine the shape of the slider—its high resolution and non-contact measurement allows the slider to be measured with the required degree of precision. The interferometer creates a map of the out of plane deflection of the slider and automatically calculates the crown, camber, and twist. To test the effect of a scribe pattern, an entire row was measured using the interferometer,

then scribed, and the row was measured again. Subtracting the two slider profiles (before and after) gives the distortion generated by the scribes.

There are several issues that affect the accuracy and repeatability of this technique. Ideally, the actual measured profile would be used to describe the shape of the slider. However, the material properties of the AlTiC prevent a repeatable profile—the alumina and titanium carbide grains have different optical properties, resulting in a profile that has a very large deviations that are not physically present (as shown in Figure 3.6). Subtracting the before and after profiles can result in amplifying these deviations,

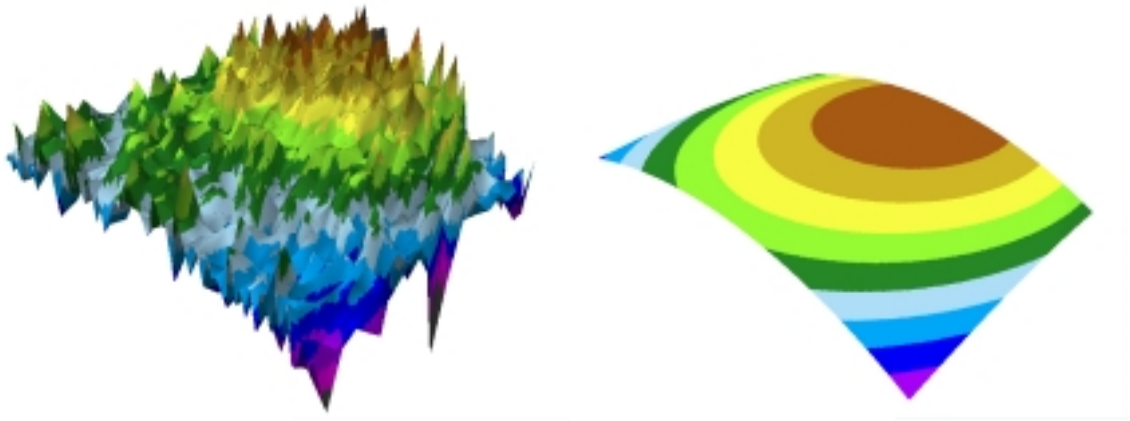

Figure 3.6. Interferometer Profile of Slider and Biquadratic Curve Fit.

which can hide the actual shape of the slider. So, the biquadratic parameters (crown, camber, and twist) are used to describe the shape of the slider. The three parameters provide the average curvature in each direction, essentially acting as a low pass filter on the data. As mentioned previously, the biquadratic curve fit removes any rigid body rotation from the data, so the curvatures found before and after scribing and can be subtracted to directly give the curvature created by the scribing pattern.

Due to the high degree of precision necessary in the measurement of the sliders, the repeatability of the measurements must be considered when collecting data. To test the interferometer, curvatures from six sliders were recorded and the sliders were removed from the interferometer. Some time later the sliders were measured again without any modifications. Table 3.1 shows the results of this test. The average repeatability of a single measurement is 0.098 nm. However, recall that to determine the

Table 3.1. Interferometer Repeatability Test

Row No.	Slider No.	Crown Change (nm)	Camber Change (nm)	Twist Change (nm)
1	10	-0.08	-0.03	0.18
1	20	0.12	-0.09	-0.09
3	10	-0.11	0.16	-0.12
3	20	0.07	-0.04	0.06
4	10	0.06	0.11	-0.17
4	20	0.05	0.14	-0.08

effects of a single scribe, measurements are required before and after a scribe. With the data scattered positive and negative, the actual determination of a scribe's effect could vary approximately ±0.2 nm. This variation is significant in determining what scribing patterns are admissible, and how many measurements are needed to have an accurate representation of the curvatures created by a scribing pattern.

3.4 Scribing Patterns

The scribing patterns used to calibrate the laser scribing model needed to encompass the LCAT's range of capabilities in scribe length, scribe location, and scribe direction. To remove any variation in scribe strength, the laser parameters (power,

frequency, and beam width) were held constant—IBM has experimented extensively with these parameters and determined an optimal setting. There are a few limitations on scribe placement and length. The scribes cannot cross—interaction effects create problems with the surface of the slider. The scribes are approximately 40 μm wide; placing an ultimate limit on scribe spacing. Also, the scribes cannot be placed too close to the edges of the slider—one edge contains the read/write electronics which are distorted by the residual stress induced by the laser scribes. To prevent creating additional twist, scribes are usually made in the *x* and *y* directions and are symmetric with respect to the other axis.

Ideally, several single scribes of varying locations and lengths would be used to calibrate the model. Experimental history at IBM shows that a single scribe creates approximately 0.6 nm of curvature in the crown direction. This level of curvature is very small considering that the repeatability of a single measurement is roughly 0.1 nm; the experiments could easily see 16% (or more) error just due to measurement repeatability. This error can be reduced by repeating the scribe pattern and averaging the results; using single scribes for calibration purposes, however, requires an impractical number of measurements. To reduce the number of required measurements, the overall deflection (and thus the number of scribes) needs to be sufficient to reduce the error. Three scribes is the minimum number of scribes to reduce the measurement error less than 10% for a single measurements; ten measurements reduces the average error to 2.5%.

Using multiple scribes for calibration raises the issue of superposition. If the scribes obey superposition, then the curvature created by a set of scribes is equal to the sum of the curvatures created by the individual scribes. Fortunately, a test for superposition is relatively simple; it consists of three patterns—two independent patterns

and a pattern that contains all of the scribes present in the other two. If the curvatures of the "superposed" pattern are the sum of the curvatures of the two independent patterns, then superposition is obeyed. This exact test was performed and the results confirmed that laser scribing obeys superposition for non-overlapping scribes (see *Experimental Results*). Since the scribes obey superposition, individual scribes can be modeled and their curvatures added to give the curvature generated by a certain scribing pattern—a versatile technique that allows a library of single-scribe solutions to represent a multitude of scribing patterns.

The set of experiments used for calibration purposes must give an accurate indication of the range of capability of the LCAT system and must be simple enough to model accurately. To accomplish this, all scribes were made in the *x* and *y* directions and were centered on the slider. Therefore, all of the calibration scribing patterns are symmetric with respect to the *x* and *y* axes, thus theoretically eliminating any twist generation. Calibration of symmetric patterns is straightforward—forces f_M and F_M (or f_m, refer to Figure 3.2) are varied until the desired crown and camber are reached.

To encompass the range of ability of the LCAT system, the patterns must show variation in scribe length and placement. For scribes in the y direction, the length can vary from approximately 600 μm to 1000 μm; any shorter and the deflections become smaller than can accurately be measured (for three 600 μm scribes, the crown is 1.6nm), any longer and the scribe interferes with the read/write head. For *x*-direction scribes, the range of scribing lengths is from approximately 350 μm to 1005 μm. Scribes can be placed at nearly any location on the slider and therefore, the minimum spacing is approximately 40 μm (the spacing where scribes start to overlap). However, spacing of *x*

scribes has a limit—the 120 μm at each end of the slider (in the *y* direction) is removed from the data set to prevent the roll-off from affecting the curvature parameters. Using this set of parameters, a calibration set was created with sixteen experiments. Table 3.2 describes the geometry of all sixteen laser scribing patterns. Note that test cases 6, 7, and 8 constitute a superposition test. This set of test cases encompasses a wide range of the LCAT's capabilities and provides adequate information to calibrate the model.

Table 3.2. Laser Scribing Calibration Test Cases

Test Case	Direction	No. of Scribes	Length (μm)	Spacing (μm)
1	*y*	3	1000	80
2	*y*	3	800	80
3	*y*	3	600	80
4	*y*	3	1000	40
5	*y*	3	1000	240
6	*y*	3	800	160
7	*y*	4	800	160
8	*y*	7	800	80
9	*x*	3	1005	80
10	*x*	3	747	80
11	*x*	3	556	80
12	*x*	3	365	80
13	*x*	3	1005	400
14	*x*	3	1005	200
15	*x*	3	1005	40
16	*x*	5	1005	200

3.5 Experimental Scribing Results

The sixteen test patterns were produced and measured using the following method:

1. *ABS sides of 44 sliders (1 row) measured and recorded using the interferometer.*
2. *Sliders loaded into LCAT, scribing patterns programmed and scribed with pauses between each slider (to prevent thermal effects).*
3. *Sliders removed from LCAT; flex sides examined under optical microscope to verify scribe placement and lengths.*
4. *ABS sides of sliders measured and recorded using the interferometer*.

Using this technique, 5 rows were scribed and measured, resulting in 215 measured sliders (five sliders were removed from the data set due to errors in scribe placement and length). Most of the scribe patterns were repeated for 11 sliders and the results were averaged to help reduce measurement repeatability errors in the calibration data. Results are shown in Figures 3.7, 3.8, and 3.9 and more detailed results are given in Table 3.3.

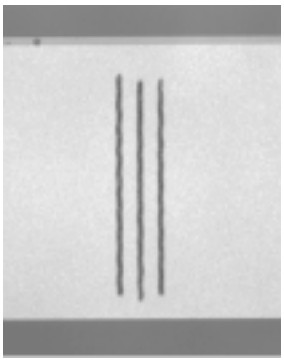

Test Case 1
3 *y* scribes
L = 1000 μm
Spacing = 80 μm
Crown: 1.65 nm
Camber: 2.65 nm
Twist: -0.05 nm

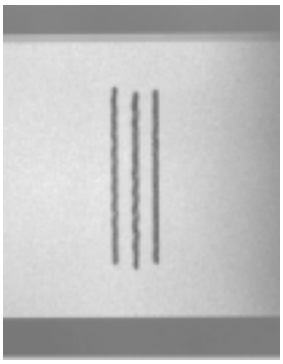

Test Case 2
3 *y* scribes
L = 800 μm
Spacing = 80 μm
Crown: 1.82 nm
Camber: 2.55 nm
Twist: 0.09 nm

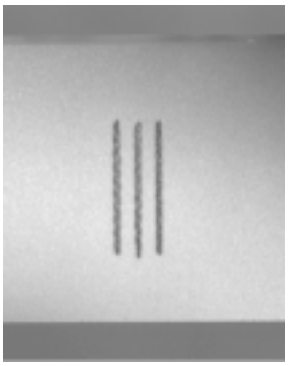

Test Case 3
3 *y* scribes
L = 600 μm
Spacing = 80μm
Crown: 1.66 nm
Camber: 1.96 nm
Twist: 0.21 nm

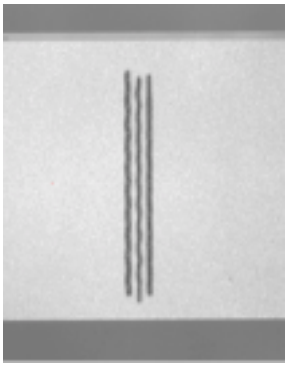

Test Case 4
3 *y* scribes
L = 1000 μm
Spacing = 40 μm
Crown: 1.58 nm
Camber: 2.54 nm
Twist: 0.02 nm

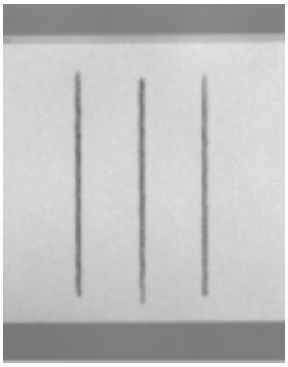

Test Case 5
3 *y* scribes
L = 1000 μm
Spacing = 240 μm
Crown: 1.56 nm
Camber: 1.83 nm
Twist: -0.03 nm

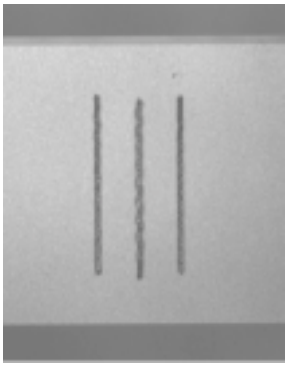

Test Case 6
3 *y* scribes
L = 800 μm
Spacing = 160 μm
Crown: 1.91 nm
Camber: 2.35 nm
Twist: 0.06 nm

Figure 3.7. Experimental Results for Test Cases 1 through 6.

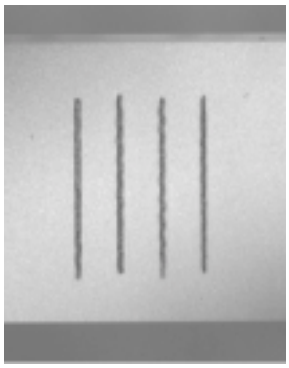

Test Case 7
4 *y* scribes
L = 800 μm
Spacing = 160 μm
Crown: 2.84 nm
Camber: 2.94 nm
Twist: -0.15 nm

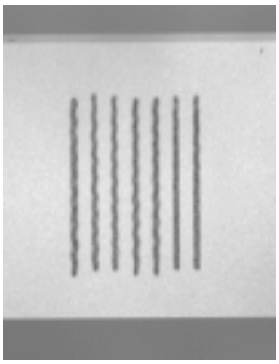

Test Case 8
7 *y* scribes
L = 800 μm
Spacing = 80 μm
Crown: 4.64 nm
Camber: 5.37 nm
Twist: -0.53 nm

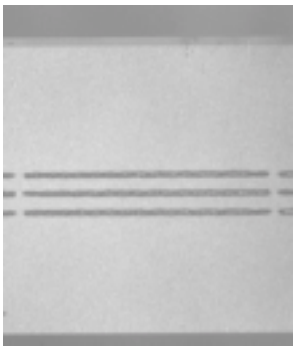

Test Case 9
3 *x* scribes
L = 1005 μm
Spacing = 80 μm
Crown: 3.69 nm
Camber: 1.59 nm
Twist: -0.27 nm

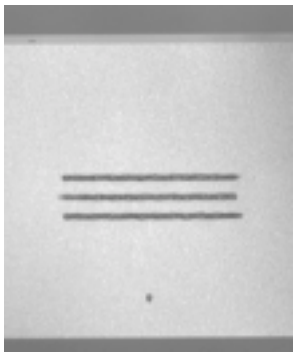

Test Case 10
3 *x* scribes
L = 747 μm
Spacing = 80 μm
Crown: 2.59 nm
Camber: 1.59 nm
Twist: 0.18 nm

Test Case 11
3 *x* scribes
L = 556 μm
Spacing = 80 μm
Crown: 1.82 nm
Camber: 1.24 nm
Twist: -0.01 nm

Test Case 12
3 *x* scribes
L = 365 μm
Spacing = 80 μm
Crown: 1.11 nm
Camber: 0.84 nm
Twist: -0.11 nm

Figure 3.8. Experimental Results for Test Cases 7 through 12.

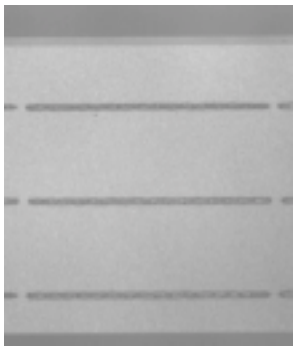

Test Case 13
3 *x* scribes
L = 1005 μm
Spacing = 400 μm
Crown: 1.75 nm
Camber: 21.72 nm
Twist: 0.07 nm

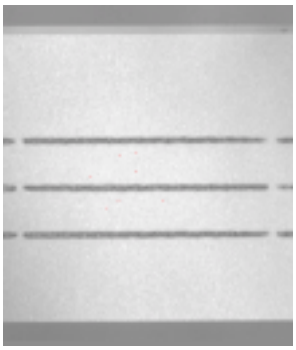

Test Case 14
3 *x* scribes
L = 1005 μm
Spacing = 200 μm
Crown: 3.07 nm
Camber: 1.69 nm
Twist: -0.03 nm

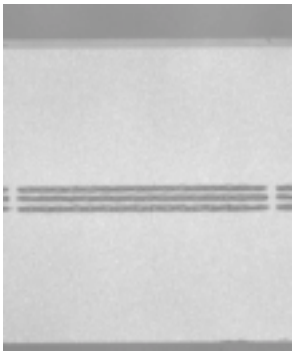

Test Case 15
3 *x* scribes
L = 1005 μm
Spacing = 40 μm
Crown: 3.66 nm
Camber: 1.56 nm
Twist: -0.51 nm

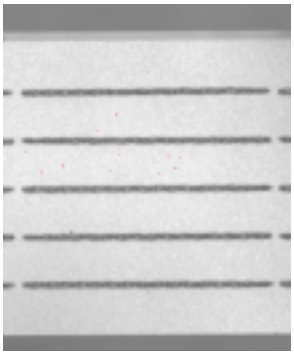

Test Case 16
5 *x* scribes
L = 1005 μm
Spacing = 200 μm
Crown: 4.17 nm
Camber: 3.23 nm
Twist: -0.44 nm

Figure 3.9. Experimental Results for Test Cases 13 through 16.

Table 3.3. Experimental Laser Scribing Data

		Curvature - Average			Curvature - Standard Deviation		
Test Case	No. Samples	Crown (nm)	Camber (nm)	Twist (nm)	Crown (nm)	Camber (nm)	Twist (nm)
1	8	1.6464	2.6527	-0.0500	0.1726	0.1764	0.1998
2	10	1.8230	2.5480	0.0910	0.1739	0.0991	0.0700
3	11	1.6573	1.9600	-0.2127	0.1106	0.0822	0.1761
4	11	1.5800	2.5373	0.0155	0.1254	0.0940	0.2267
5	11	1.5573	1.8273	-0.0345	0.0855	0.0413	0.1882
6	7	1.9114	2.3457	0.0571	0.0871	0.0640	0.1751
7	7	2.8414	2.9443	-0.1514	2.5020	0.1336	0.3235
8	7	4.6371	5.3686	-0.5314	0.3661	0.2746	0.3321
9	11	3.6873	1.5909	-0.2700	0.2050	0.1015	0.3814
10	11	2.5873	1.5855	0.1764	0.2098	0.0805	0.2948
11	11	1.8209	1.2418	-0.0127	0.1487	0.0540	0.1851
12	11	1.1082	0.8373	-0.1091	0.0672	0.0307	0.1283
13	44	1.7470	1.7218	0.0661	0.2977	0.1417	0.3841
14	11	3.0745	1.6900	-0.0318	0.2934	0.0621	0.4065
15	11	3.6573	1.5609	-0.5109	0.2096	0.1188	0.4393
16	11	4.1709	3.2345	-0.4400	0.3622	0.2631	0.3887

*Note: See Table 3.2 for scribing geometries

Examination of the data reveals some interesting conclusions (both about metrology and the scribing results). The standard deviations are on the order of 0.10 nm —very close to the uncertainty predicted by the repeatability experiment, meaning that the laser scribes themselves are consistent and repeatable within the measurement error. The presence of small amounts of twist in the data indicates that the scribes may not have been completely symmetric with respect to the *x* and *y* axes or the scribing geometry is not as simple as once thought. The raw data (given in Appendix B) indicates that the test cases showing the most twist were performed on rows that were highly twisted before scribing—the twist could possibly be generated because the scribes are placed on an asymmetrically curved surface. Furthermore, the average value of twist and the standard deviations for all three curvatures can be reduced by removing the sliders from the end of the rows from the data set. For example, if the first slider from Test Case 10 is removed,

the twist drops from 0.1764 nm to 0.1150 nm and all three standard deviations decrease. The inconsistent data from the end of the rows is a result of varying boundary conditions—the sliders in the middle of the row have other sliders (with similar scribing patterns) on both sides, but the sliders on the end have a free edge. The different boundary conditions can cause inconsistency in results—a point further demonstrated by the finite element models used to model the laser scribing. However, the experimental data does show that the laser scribing process is consistent and relatively repeatable across the range of operation of the LCAT system. Therefore, the experiments represent a good calibration set for the laser scribing model.

4 Finite Element Modeling

4.1 Background

A robust model of any scribing system must be capable of accurately modeling any scribing geometry. Analytical models can produce accurate results for mechanical scribes in simple geometric patterns (see Sections 2.1 and 2.2). Applying this type of analytical solution to mechanical scribes with finite lengths is impractical. Furthermore, all proposed laser scribing models (see Section 3.1) require finite length scribes and generate end effects. So, a flexible and accurate numerical technique was sought that allows three-dimensional solutions of any scribing geometry.

Finite element analysis offers geometric flexibility and high accuracy with proper considerations. For the scribing models, a basic linear elastic finite element analysis was chosen because three dimensional elasticity has previously been used to accurately model residual stresses (Ahn (1993)) and it allows fast and accurate solutions. The technique relies on elements that represent differential units, assembled into a mesh that represents the overall geometry. A large system of equations represents an approximation to the actual elasticity solution. The solution converges as the number of elements increases.

The construction of the mesh is critical in the accuracy of the finite element analysis. Increasing the number of elements improves accuracy, but increasing the number of elements can rapidly increase the solution time and the amount of computational power needed. However, proper selection of element size and placement can improve accuracy without drastically affecting computational time. If the mesh density (the size and number of elements in a given region) is high in the regions of high

stress, the accuracy of the model can be improved. Scribing creates a very localized stress field (as shown in Figure 2.5) that requires a very high mesh density near the scribe. However, the stress is negligibly small a short distance from the scribe, and the mesh density can be rather coarse without affecting accuracy. Also, careful use of symmetry allows a reduction in the number of elements used by a factor of two without adding any additional elements or affecting computational time. Taking these facts into consideration, the desired accuracy can be achieved with the minimum required computational time.

One major consideration during the development of any finite element model is the boundary conditions. Finite element models require constraints to confine the solution of the model. In this particular case, the actual sliders are scribed as a row, and the row itself has no obvious constraints. So, the boundary conditions placed on the finite element model must eliminate all of the rigid body motions (translations and rotations) but not over-constrain the model (such that the boundary conditions influence the solution). To accomplish this task, a set of boundary conditions known as a Kelvin coupling is employed. Figure 4.1 shows the coupling as a theoretical model. Point 1 is restrained from translation in all three directions, point 2 is restrained in *y* and *z*, and point three is restrained in *z*. This set of boundary conditions restrains the body from all six rigid body motions but allows the body to elastically deform without causing any stress. These no-stress boundary conditions are critical in accurately modeling the scribed sliders, so the Kelvin coupling is used on all of the finite element models used in this project.

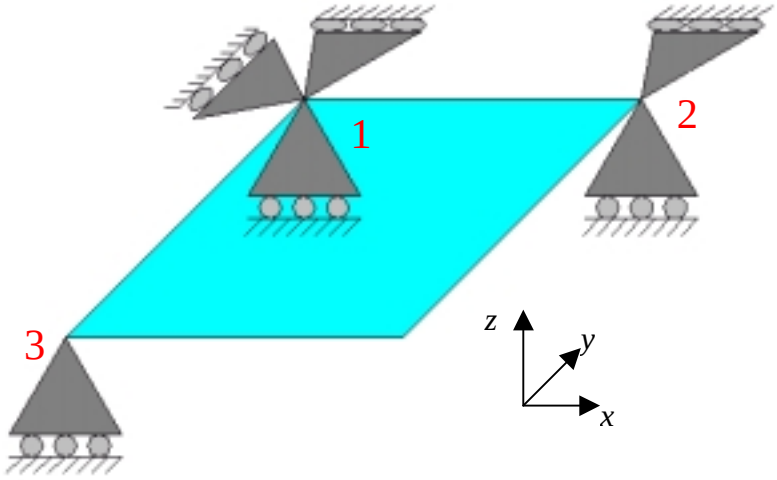

Figure 4.1. Kelvin Coupling Boundary Conditions

Mechanical scribing has been extensively discussed in Chapter 2, with the finite element modeling addressed in Sections 2.2 and 2.3. However, the bulk of the finite element work was conducted on laser scribing. The following work discusses the development of the laser scribing model and its calibration.

4.2 Laser Scribe Force Model Specification

The experimental results in Section 3.5 show that laser scribes generate curvature parallel and perpendicular to the scribe. Qualitatively, both the line force and the end force models (discussed in Section 3.1) produce deflections similar to those seen in the experimental results. To determine which model best fits the experimental data, a single slider finite element model was created to model scribes along the *y* direction. The model employs symmetry across the *y*-axis to conserve elements, and uses the Kelvin coupling placed on the corners of the slider for boundary conditions. Scribing patterns matching

those performed experimentally were modeled using both the line force and the end force systems.

The single slider model uses the techniques discussed in Section 4.1. The scribe region is 0.25 mm wide, with 24 elements spanning its width. Four elements are placed between the line forces, giving a dipole separation of 50 μm. There are 20 elements across its width, allowing scribes of 600, 800 and 1000 μm (three scribe lengths used in the experiments) to be modeled easily. Figure 4.2 shows the finite element model with the 1000 μm scribe. Note the coarse mesh outside of the scribe region—reducing the size

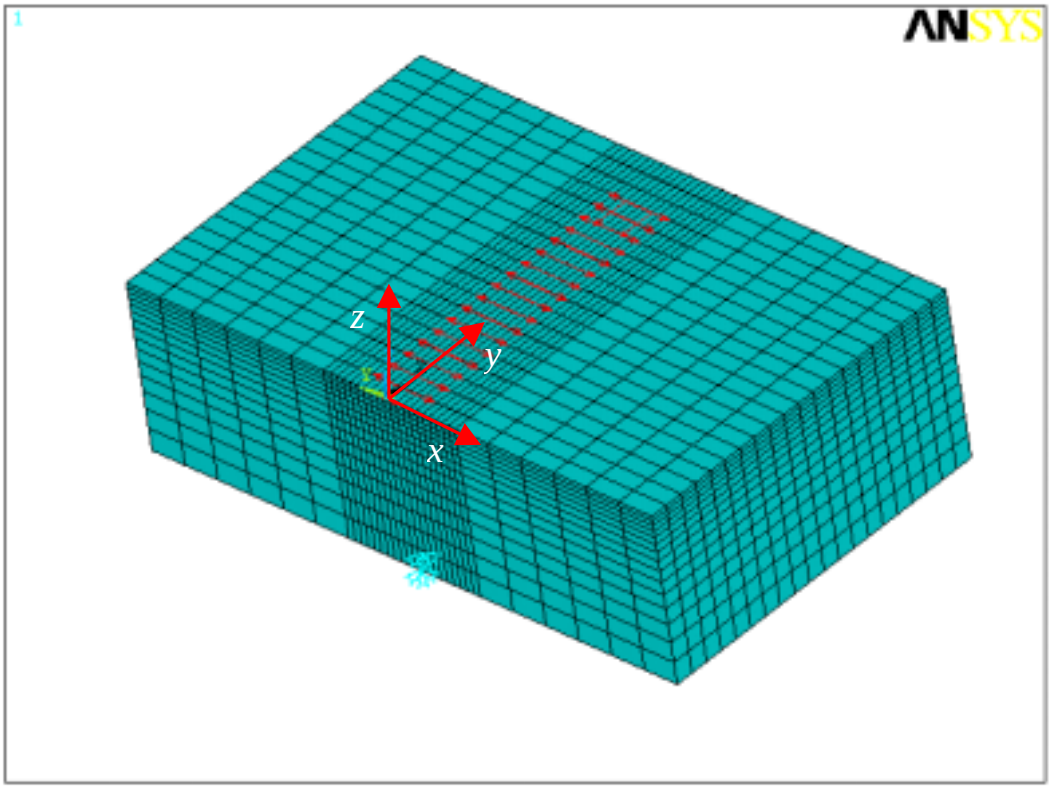

Figure 4.2. Single Slider *y*-Scribe Mesh

of the model without impacting the accuracy of the solution. The scribing region can be

moved from three single-scribe models can be superposed to give the solution for a single three-scribe model (simulating one of the experiments).

To compare the finite element solutions to the experimental results, the ABS side of each model is fitted with a biquadratic and the crown, camber, and twist are computed (in this case, twist is geometrically eliminated). The curvatures can be added for the three models representing the experimental scribes giving a total crown and camber for the model. The finite element model has not been calibrated—so the solution will not exactly match experimental results. However, the model is linear, so if the crown to camber ratio is correct, it is a simple matter of using a linear scaling factor to obtain the correct deflections.

The end force and the line force systems were applied to the finite element model using the following guidelines. The line dipoles were applied with 50 μm spacing, with a magnitude of f_M = 20 N/mm. The magnitudes of the line forces (f_m) and the end forces (F_m) were varied until the crown to camber ratio of a specific model matched that of the experimental results to a reasonable degree of precision. The modulus of elasticity was taken to be E =1 N/mm^2(the results, however, can be scaled linearly) and Poisson's ratio was taken to be 0.2. The model used for calibration is Test Case 1, consisting of three 1000 μm, y-direction scribes with a spacing of 80 μm. The experimental results gave a crown of 1.65 nm and 2.65 nm of camber, for a crown to camber ratio of 0.623. Varying the f_m in the line force model, gave a crown to camber ratio of 0.616 for Test Case 1 (a 1.11% error) with f_m = 1.50 N/mm. Using this line force as the calibration, Test Cases 2 through 8 were computed using similar models. The results are shown in Table 4.1. The model provides excellent results for the scribing patterns with 1000 μm scribes, but the

error increases as the scribe length is decreased. It is interesting to note that the error is relatively consistent for any given scribe length—an important indication that the line dipole model (that generates camber in this case) produces accurate results but the line forces do not accurately represent the stresses generated parallel to the scribe.

Table 4.1. Line Force System Calibration for *y* Scribing Models

	Finite Element Model			Experimental	
Test Case	Crown	Camber	Ratio	Ratio	% error
1	136.01	220.92	0.616	0.623	1.18
2	84.43	173.26	0.487	0.714	31.75
3	50.16	136.54	0.367	0.847	56.63
4	135.95	226.73	0.600	0.622	3.60
5	137.01	164.08	0.835	0.852	1.99
6	84.37	156.04	0.541	0.813	33.49
7	112.38	183.42	0.613	0.966	36.57
8	196.75	339.46	0.580	0.864	32.92

Performing a similar calibration for the end force model gives a crown to camber ratio of 0.615 for Test Case 1 (1.32% error) for an end force of F_m = 0.82 N. Performing the rest of the analyses for Test Cases 2 through 8 gave the results shown in Table 4.2. The results show that the end force model is quite accurate for modeling the y-direction

Table 4.2. End Force System Calibration for *y*-scribing Models

	Finite Element Model			Experimental	
Test Case	Crown	Camber	Ratio	Ratio	% error
1	130.96	213.03	0.615	0.623	1.32
2	124.42	164.59	0.756	0.714	5.87
3	108.17	128.19	0.844	0.847	0.37
4	130.92	218.66	0.599	0.622	3.74
5	131.58	157.88	0.833	0.852	2.18
6	124.48	147.66	0.843	0.813	3.69
7	166.01	172.63	0.962	0.966	0.45
8	290.49	320.29	0.907	0.864	4.97

scribes—over all eight of the test cases, the maximum error is less than six percent.

Further insight into the validity of the end force model can be obtained by examining the process by which the residual stress is created within the material. The laser scribe is actually a collection of overlapping "dots" that are created by melting the surface material with a pulsed laser. Figure 4.3 illustrates this process. A single dot of

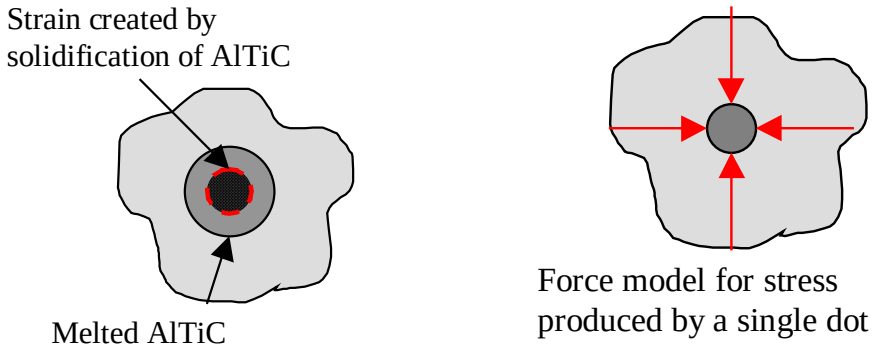

Figure 4.3. Mechanism and Model for Creation of Residual Stress by Laser Scribing

material is melted by a laser pulse, and the solidification (and the resulting contraction) of the melted material produces a strain on the bulk of the slider. The resulting residual stress is tensile in the region immediately surrounding the scribe. A simple force model

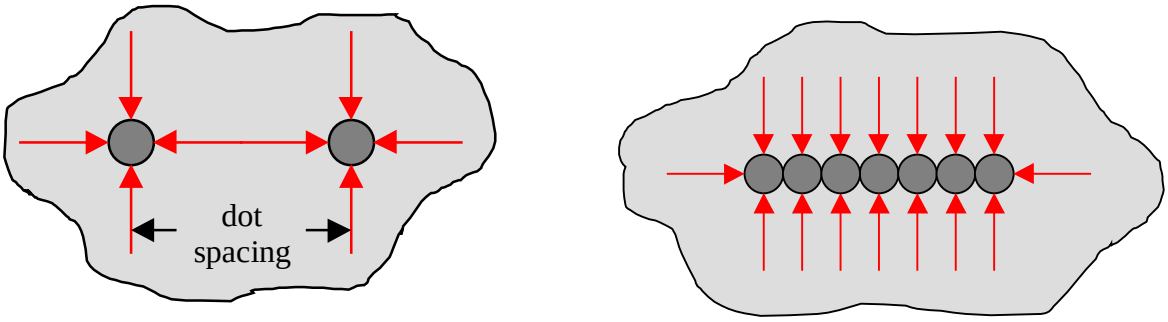

Figure 4.4. Superposition of Dot Models Yielding End Force Model for Laser Scribes

(shown in Figure 4.3) can be used to model the residual stresses produced by the solidification, similar to the indentation model proposed by Yoffe (1982). As these dots

are placed closer and closer together, the stress fields produced by each individual dot begin to overlap. The tensile forces begin to cancel one another, as illustrated in Figure 4.4. Eventually, the dot spacing is reduced to the point where the dots begin to overlap and the stress along the scribe is completely cancelled, except for the stress produced by the last dot on each end, resulting in a force system resembling the end force system.

4.3 Single Slider Models

The initial attempt to model the scribing process focused on finite element models of single sliders. The finite element meshes modeled a slider measuring 1.25 mm by 1.0 mm by 0.3 mm, employing a symmetry plane to reduce the number of elements. The scribes, as with the test cases, were limited to the *x* and *y* directions, so two adaptable meshes were developed—one for *x*-direction scribes (shown in Figure 4.5) and the other for *y* scribes (shown in Figure 4.2).

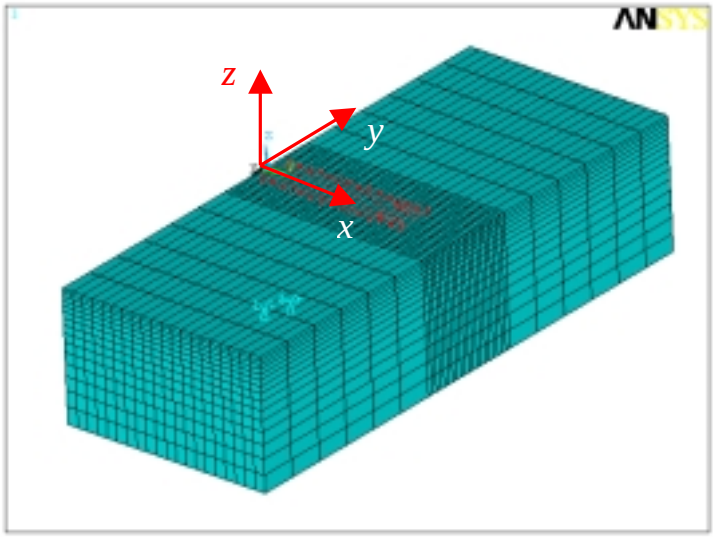

Figure 4.5. Single Slider *x*-direction Scribe Model

The two finite element meshes utilize the same techniques that were discussed in Section 4.1 for providing accurate solutions with minimal computation time. Both meshes employ symmetry planes on the centerline (the *x*-axis for the *y* scribe model and the *y*-axis for the *x* scribe model) to reduce the number of elements without impacting the accuracy of the solution. Also, the scribing region of both meshes is 0.25 mm wide, is divided up into 24 elements along its width, and the dipole separation is set at 4 elements (or 50 μm). Through the use of input file structures, the scribing region can be translated to give the scribe a different placement without drastically altering the mesh. These two meshes, with minor modifications, were used to model all 16 test cases.

The end force system was chosen to model the scribes, based on the sample calibrations (shown in Section 4.2) which yielded very accurate results for the *y*-scribe models. The calibration used to generate the data in Table 4.2 (F_m = 0.82 N) was used to model the x-scribes. The results for test cases 9 through 12 are shown in Table 4.3. The

Table 4.3. Results of FEA for *x*-scribes with F_m = 0.82 N.

	Finite Element Model			Experimental	
Test Case	Crown	Camber	Ratio	Ratio	% error
9	247.84	95.01	2.608	2.311	12.86
10	197.16	97.80	2.016	1.708	18.04
11	146.32	87.96	1.663	1.444	15.18
12	95.59	63.82	1.498	1.262	18.70

errors are much higher than in the *y*-scribe case, however, the results are closely grouped together. If the *x*-scribe models are calibrated as an independent set, the errors can be significantly reduced. A re-calibration with test cases 9 through 12 yielded an end force of F_m = 0.925 N. The data is shown in Table 4.4. The maximum error is now approximately 5%, a reasonably acceptable value.

Table 4.4. Results of FEA for *x*-scribes with F_m = 0.925 N.

	Finite Element Model			Experimental	
Test Case	Crown	Camber	Ratio	Ratio	% error
9	243.37	111.08	2.191	2.311	-5.20
10	193.89	113.40	1.710	1.708	0.10
11	144.04	101.50	1.419	1.444	-1.74
12	94.22	73.46	1.283	1.262	1.64

The need for separate calibrations depending on scribe direction raises some interesting issues. Theoretically, if the model perfectly matched the experimental conditions, a single force system (with a single calibration) would be able to model any scribing geometry. However, in the development of this model, many assumptions were made to make the modeling simple and flexible. The most obvious assumption relies on the force model itself—the actual mechanism for distortion is a melt/solidification process that produces residual stress. The force model provides a simple and possibly accurate approximation to the residual stress, but it does not work from first principles and therefore, can be a source of inaccuracy or approximation. Another assumption is that the AlTiC material is elastic and isotropic. One possible explanation for the inconsistency in results between the two directions is that the processing of the material gives it different properties in the *x* and *y* directions—the sliders are come from a 125mm diameter (1.2 mm thick) wafer that is sectioned and lapped to form the rows. Also, there is the thin layer of electronics covered by a thin (50 μm) layer of alumina on one edge—however, the material properties of alumina are very close to that of AlTiC, so very little error would be expected

The geometry of the heads themselves leads to several more assumptions. All of the finite element models are exactly 1.25 mm by 1.0 mm by 0.3 mm, but while the

actual rows and sliders do very slightly (+/- 1%). Also, the models assume that the slider is initially flat, but experimental metrology shows that the heads have a peak to valley deviation of 5 to 10 nm before scribing—the amount of deflection comparable to 3 or 4 scribes. The most obvious geometric assumption is modeling a single slider—as stated previously, all the sliders were scribed and measured as part of a 44-slider row (see Figure 3.3). This assumption produces incorrect boundary conditions on two edges of the slider, something that could effect certain scribing arrangements more than others, possibly producing considerable error.

Addressing these assumptions shows possible room for improvement in the model to produce more accurate results. First, it is important to note that the calibration values obtained through experimentation are not exact—there is a reasonable margin of error (approximately 10%) in every curvature measurement and the averaging effect only brings down the margin of error to approximately 2%. Therefore, improving the accuracy much beyond the +/- 2% error region is impossible, so assumptions that have very small effects can be left alone. That said, little is known about the actual melt/solidification process that occurs when a laser scribe is produced, therefore trying to model the scribing from first principles would change the scope of the project and possibly produce no better results. The material properties of the AlTiC are not well known, and they are also highly dependent on the batch and the manufacturer (IBM currently uses three suppliers with their own techniques for manufacturing AlTiC wafers). The actual size and pre-scribed shape of the sliders also depends on the specific batch of sliders and the polishing process they have undergone—therefore any experimental work to determine slider sizes and material properties would only be

specific to the individual sliders that were experimented with. However, *all* sliders are scribed as a part of a row—and the difference in boundary conditions between a single slider and a slider as a part of a row could make a significant difference in the solution. This effect is most obvious with the x-direction scribes that are 1000 μm in length. The model has these scribes extending all the way across the slider, so there are some interesting edge effects that occur on the sides of the slider (see a plot of the principal stresses given by the ANSYS model in Figure 4.6). Note the two displacement peaks

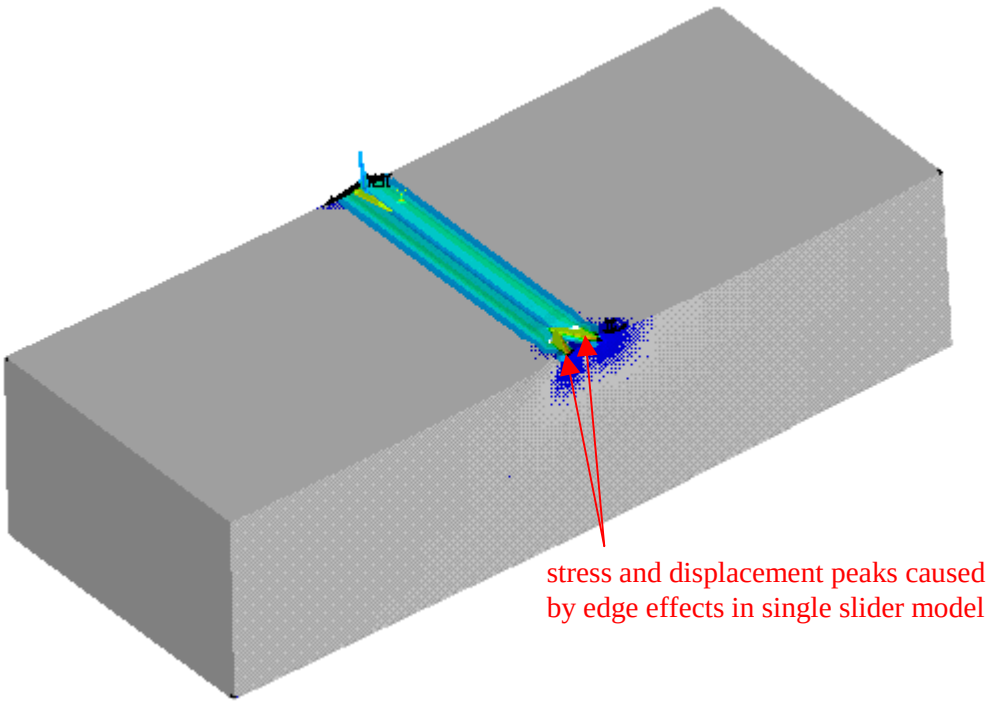

Figure 4.6. Principal Stresses for Single Slider Model of a 1000 μm *x*-scribe

caused by the end forces on the edge of the slider. However, in actuality, the scribes do have terminal points, and do not overlap with the scribe on the neighboring slider (as shown in Figures 3.8 and 3.9 with test cases 9, 13, 14, 15, and 16). Compensating for

these boundary conditions could give significant improvement in the accuracy of the results.

Modeling an entire row of 44 sliders is impractical and unwieldy—single slider models take approximately 20 minutes to complete on a relatively fast personal computer, and 22 models must be completely analyzed to check all 16 test cases for calibration. However, an improvement can be made over the single slider model by modeling three sliders—the center slider has the correct boundary conditions and should yield more accurate results.

4.4 Three Slider Models

The single sliders models yielded accurate results for most of the calibration scribing patterns; however, in patterns where the scribes extended near the edges along the *x*-axis, the models became more inaccurate due to an inconsistency between the experimental and theoretical boundary conditions. To account for this effect, finite element meshes of three connected sliders were constructed—the center slider offers the correct boundary conditions and should show an improvement in accuracy.

The construction of the three-slider finite element meshes utilized many of the techniques shown in the single slider models, but it required some compromises due to computational limitations. The Kelvin coupling and the finely meshed scribing region were carried over, but to eliminate any conflicts with boundary conditions and application of forces, the symmetry planes were removed so that the entire region is meshed. Meshing the entire region with identical mesh density and element placement as

in the single slider model resulted in a mesh with six times as many elements, which requires an impractical amount of computer resources. To reduce the number of elements, the mesh density in the model must be decreased; a technique which can reduce the accuracy of the finite element model if not done properly (see Section 4.1). To keep the mesh density high around the scribe, the meshing of the scribing region remained nearly the same—the same 24 elements over the 0.25 mm span. However, the number of elements across the thickness of the slider was changed from 15 to 10. The gradient placed on the meshing of the thickness allowed the first few elements (which contain most of the stress field) to remain nearly the same size. The change in the meshing of the thickness made a considerable reduction in the number of elements required, making the three-slider model feasible with the computational resources at hand.

The number of elements along the scribing axis had several considerations in addition to mesh density. The single slider models utilized 20 elements across half of the length or width of the slider (depending on scribing direction)—reproducing this mesh density in the three slider models results in a large number of elements. Reducing the number of elements does not impact accuracy appreciably, but it does create problems with producing the correct scribing lengths. With single scribes, there were enough elements to model the correct scribe lengths to within 2% without altering the mesh. However, with a coarser mesh, modeling the scribes with a single mesh is difficult (especially the *x* scribes, which have lengths of 365, 556, and 747 μm). So for each scribe length, a new mesh was made that allowed the length of the force model to match the scribe. Table 4.5 shows the number of elements in the scribe direction—to interpret

the table, recall that the individual slider width (x direction) is 1.068 mm, and the slider length (y direction) is 1.25 mm.

Table 4.5. Mesh Specifications for Scribes on Three Slider Models

Direction	Actual Length (μm)	No. Divisions per Slider	No. Divisions per Scribe	Modeled Length (μm)
x	365	15	5	356
x	556	17	9	565
x	747	20	14	748
x	1005	30	28	997
y	600	23	11	598
y	800	22	14	796
y	1000	20	16	1000

Using these specifications, the number of elements was dramatically reduced, resulting in the three-slider models being 50% larger than the single slider models (as opposed to 500% larger if the mesh density was completely duplicated). Figures 4.7 and 4.8 show the meshes for a 747 μm *x*-scribe and a 1000 μm y-scribe, respectively.

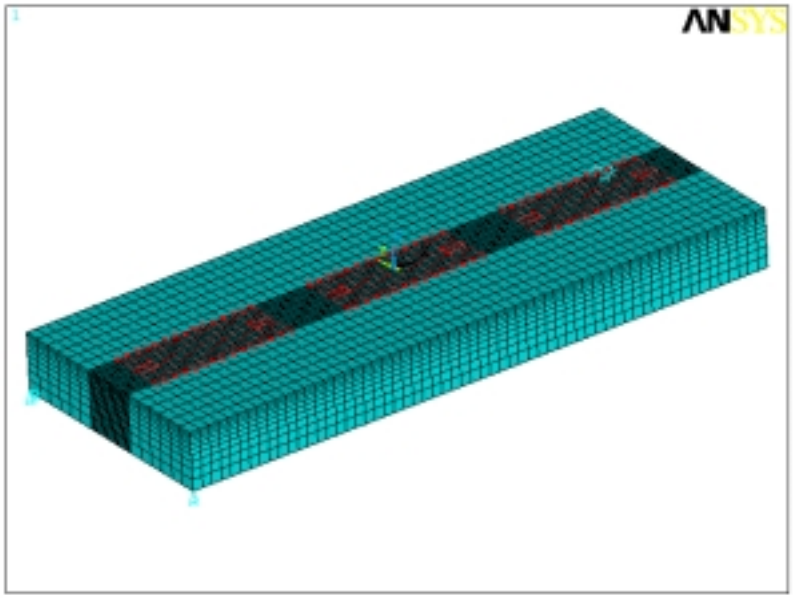

Figure 4.7. Finite Element Mesh for 747μm *x*-direction Scribe

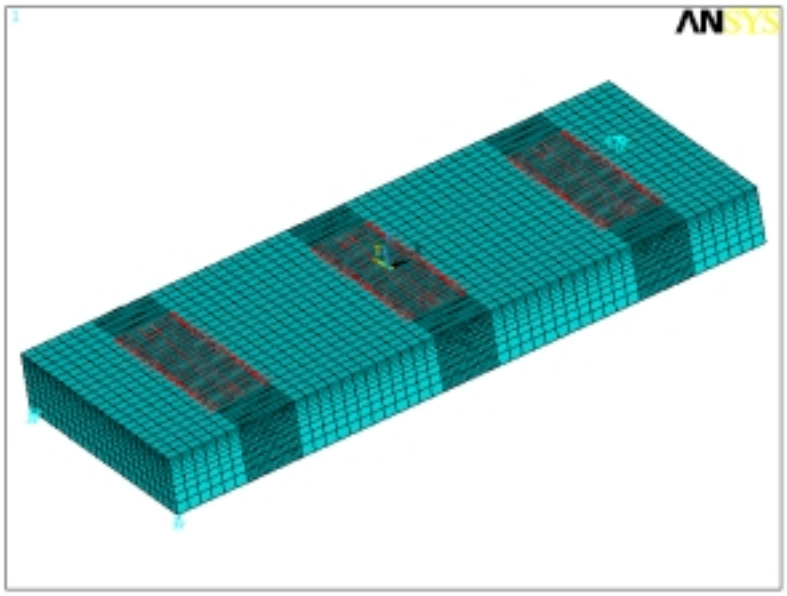

Figure 4.8. Finite Element Mesh for 1000 μm *y*-direction Scribe

The scribing force models were applied in a similar manner to the single slider models. The line forces were applied with magnitude f_M = 10 N/mm and the end forces were varied to calibrate the model to the correct crown to camber ratio. Note that the force models were applied identically to each of the sliders to best simulate the experimental conditions. Using a similar procedure to the single scribe models, a calibration for the *x* and *y* scribes were generated. Test cases 1 through 8 were used for the *y* scribe calibration and cases 9 through 12 for the *x* scribes (cases 13 though 16 require special consideration and were dealt with separately).

Table 4.6 shows the results for the calibration for the y-direction scribes. Using an end force of F_m = 0.248 N, the eight test cases were calibrated such that the overall error was minimized. Note that the average deviation is 2.02% with the maximum error being 3.35%. The three-slider model offers slight improvement over the single slider model in accuracy, which had an average deviation of 2.83% and a maximum error of 5.87% (see Table 4.2).

Table 4.6. Three Slider Model *y* Calibration (F_m = 0.248 N)

	Finite Element Model			Experimental	
Test Case	Crown	Camber	Ratio	Ratio	% error
1	37.84	61.10	0.6193	0.6207	-0.22
2	35.98	48.66	0.7394	0.7155	3.35
3	30.86	36.61	0.8428	0.8456	-0.32
4	37.85	62.72	0.6034	0.6227	-3.11
5	37.80	45.64	0.8282	0.8522	-2.82
6	35.97	43.74	0.8222	0.8149	0.91
7	47.93	51.39	0.9327	0.9651	-3.35
8	83.90	95.13	0.8819	0.8637	2.10

The *x*-direction scribes (test cases 9 through 12) are shown in Table 4.7. The *x*-scribes were calibrated separately (using a single calibration shows results similar to the single slider models), and an end force of F_m = 0.227 N gave the best calibration for the four test cases. The average deviation for the *x*-scribe models is 4.7%, with a maximum deviation of 9.1%. The three-slider model is ***less*** accurate for *x* scribes than the corresponding single slider model. Investigation into the construction of the model yielded some of the sources of inaccuracy.

Table 4.7. Three Slider Model *x* Calibration (F_m = 0.227 N)

	Finite Element Model			Experimental	
Test Case	Crown	Camber	Ratio	Ratio	% error
9	60.66	28.72	2.1118	2.3240	-9.13
10	46.54	27.93	1.6662	1.6319	2.10
11	36.26	25.98	1.3956	1.4663	-4.83
12	24.66	18.14	1.3596	1.3235	2.72

The maximum error exhibited by the *x*-scribe model occurred with test case 9—three scribes of length 1005 μm. This same scribing pattern generated the most inaccurate results for the single slider model because of the inability of the model to capture the stress field created by the scribe (due to an inconsistency in boundary

conditions). The three-slider pattern was devised to correct this inconsistency, but the results do not show improvement. However, closer examination of the mesh for the *x*-direction, 1005 μm scribes reveal the possible problem.

The elements used in this analysis only allow the stress to vary linearly across an element edge. In the 1005 μm, *x*-scribe case, there are only two elements between the ends of the scribes on the adjacent sliders. The stress field is rapidly changing around the endpoints of the scribe, so approximating it by two linear segments will not yield accurate results. The crown to camber ratio being too high confirms this—the end forces control camber in the *x*-scribe case, so if the stress field were more accurately represented, the camber would increase, producing a more accurate result. To remedy this modeling problem, a new mesh, shown in Figure 4.9, was constructed for this

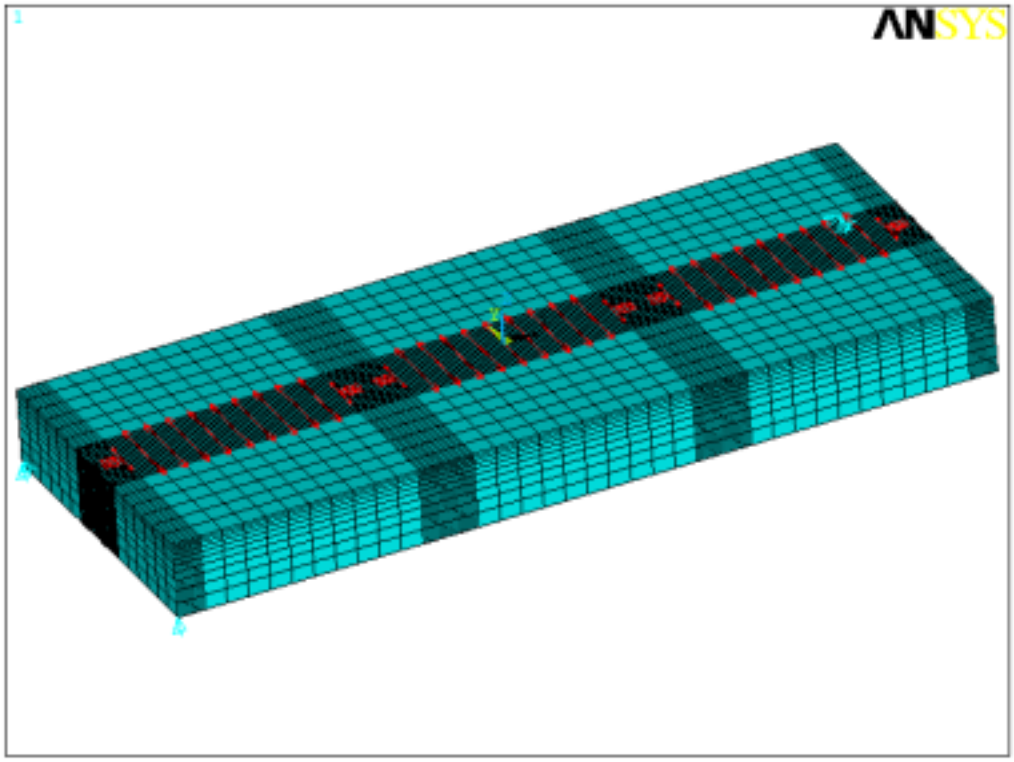

Figure 4.9. Finite Element Mesh for 1005 μm *x*-direction Scribes

specific case. The mesh has a finely meshed region at the edge of each slider, consisting of 10 elements over a span of 0.1068 mm. Using this mesh, the end force system can be applied and there are six elements in between the end forces, allowing a more accurate determination of the stress field in that region. The force system is applied in the same manner—although, applying f_M = 10 N/mm require careful consideration when the element size changes.

Using ANSYS to find the solution to the finite element model shows that the specialized mesh did a much better job of capturing the stress field. The new mesh resulted in a distinct separation of the stress fields created by the two adjacent scribes—experimental results indicate that the laser scribes produce very localized stresses, so this separation most likely occurs in the stress field in the laser scribed sliders. The original model for this scribe shows no separation between the stress field of the scribes and the error in the crown to camber ratio indicates that the end forces were not producing enough camber (as compared with the experimental results).

Using the new mesh, test cases 9 through 12 were re-calibrated and the results are shown in Table 4.8. The new calibration has a slightly smaller end force (F_m = 0.213 N

Table 4.8. Three Slider Calibration for *x*-Scribes with Revised *x*-1005 Model (F_m = 0.213 N)

	Finite Element Model			Experimental	
Test Case	Crown	Camber	Ratio	Ratio	% error
9	61.34	26.40	2.3238	2.3240	-0.01
10	45.73	26.64	1.7167	1.6319	5.20
11	34.60	23.84	1.4516	1.4663	-1.01
12	21.80	17.19	1.2681	1.3235	-4.19

instead of 0.227 N), resulting in different errors for each of the cases. For this new

calibration, the average deviation from the experimental results is 2.6%, with a maximum error of 5.2%--an improvement over the previous average and maximum of 4.7% and 9.1%, respectively. This calibration brings the accuracy of test cases 9 through 12 to a similar level as the y calibrations (test cases 1 through 8).

Test cases 13 through 16 presented some unusual problems that were addressed only when considering experimental technique. All four cases are 1005 μm scribes in the *x*-direction, with varying spacing. Using the calibration given in Table 4.8 and the finite element mesh shown in Figure 4.9, the four scribing patterns were modeled and the results are shown in Table 4.9. The accuracy of the models varies considerably,

Table 4.9. Three Slider Models for Test Cases 13 Through 16 (F_m = 0.213 N)

	Finite Element Model			Experimental	
Test Case	Crown	Camber	Ratio	Ratio	% error
13	33.32	26.38	1.2629	1.0146	24.47
14	54.18	26.40	2.0525	1.8192	12.83
15	62.41	26.40	2.3639	2.3431	0.89
16	66.58	43.98	1.5138	1.2895	17.40

depending on the spacing and placement of the scribes. Test case 15 (3 1005 μm scribes with 40 μm spacing) shows excellent accuracy, but as the scribing spacing increases, the accuracy deteriorates to nearly 25% error at 240μm spacing. After careful examination of the models and the experimental technique, an explanation was found for the errors for these large spacings. When performing the measurements with the interferometer (see Section 3.3), a region at the top and bottom of each slider is removed from the scan to eliminate edge effects caused by the electronics or the polishing processes. So, for test cases 13, 14, and 16, the scribes are placed very close to this region, so some of the deflection created by these scribes is removed from the data collected, resulting in

erroneous crown and camber measurements. This effect produces very little error in cases where the scribe does not come close to this region, such as test cases 9, 10, 11, 12, and 15 and all of the y-scribing patterns. When using this model to predict the crown and camber of a scribing pattern, careful consideration must be given to prevent error caused by this “roll off” effect.

4.5 Numerical Considerations and Comparisons

Both the single slider and three slider models can reasonably accurately predict the curvatures produced on a given slider by a laser scribe pattern. Currently, the three crown, camber, and twist curvatures are the only parameters used to characterize the shape of the slider due to measurement limitations (see Section 3.3 for an explanation). However, as technology is improved, the actual shape of the slider could be of consequence.

The single and three slider finite element models have distinctly different boundary conditions and calibrations to produce similar curvature predictions. These curvature predictions, however, are just the result of the biquadratic fit to the actual surface shape. The actual shape of the models varies significantly while yielding the same crown camber and twist. Figure 4.10 shows the shape of the ABS side of the calibrated single and three slider models for a single centered 800μm scribe in the y-direction. The plots are on the same vertical scale, so the peak to valley measurement is comparable for the two cases, but there are several important differences between the models. The single slider result exhibits more gradual curvature in the x and y directions. Also, the terminal curvatures on the x and y edges are higher for the single slider case.

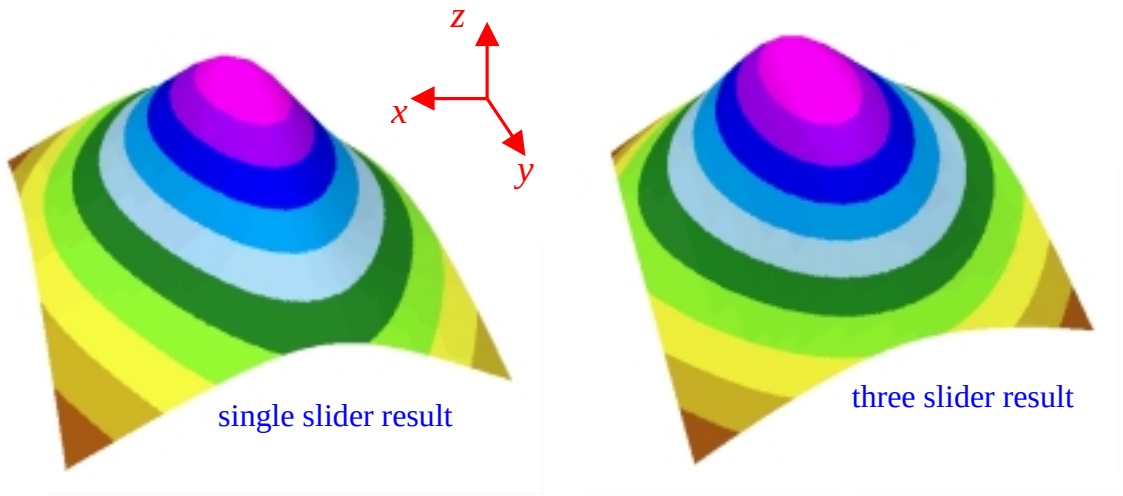

Figure 4.10. Comparison Between Shapes Produced by Scribing Single and Three Slider Models with an 800 μm *y*-scribe

The difference in boundary conditions causes most of this effect—the three slider result is forced to match displacement and slope with a similar slider on each *y*-*z* face, while the single slider has free boundaries. This difference can be illustrated by the comparing the three sliders in the three slider model—the first and third sliders have one free end and one joined end, while the center slider has two joined ends. Taking the same sample case (a single 800μm scribe in the *y*-direction), the first and third sliders have a crown and camber of 10.923 and 16.953, respectively. The center slider has a crown of 10.988 (a difference of 0.59%) and a camber of 16.958 (a difference of 0.03%). The variation in crown and camber is significant (for calibration), but there is also a difference between the slope on the free edge and the joined edge. This variation also offers an explanation for the inconsistency in the experimental data for the sliders on the ends of the rows (see Section 3.5).

The three slider models have demonstrated the ability to predict the shape generated by a scribing pattern with a high degree of accuracy. Using the finite element

results, the models can be scaled to determine the actual deflection created by a laser scribe pattern on the AlTiC rows. With a fully calibrated model, the curvatures produced by an arbitrary scribing pattern can be predicted.

5 Results

5.1 Calibration for Deflections

The calibrations in Chapter 4 show that the laser scribe force model can accurately predict the *shape* of the deflected slider, but the calibrations so far have not addressed the actual magnitude of the curvatures. Theoretically, this is a simple matter—the finite element analyses are linear, so the results can be scaled linearly to reflect changes in material properties and loading (recall that the slider is assumed to be isotropic). Thus, in principle, calibrating the model requires a ratio of the end force to the line force (found in Chapter 4) to establish the crown to camber ratio, then a constant to establish the magnitude of the curvatures.

Calibrating the crown to camber ratio of the *y*-scribes was performed in Section 4.4 (results shown in Table 4.6). Calibrating the deflections requires the introduction of a multiplier constant (called *C* in the following analyses) that scales the results of the finite element analyses to match the experimental results. The constant *C* was varied until the experimental and predicted camber for Test Case 1 were equal, resulting in $C = 0.04342$.

Table 5.1. Full Calibration for *y*-scribes ($C = 0.04342$)

	Crown			Camber		
Test Case	Experimental	Predicted	% error	Experimental	Predicted	% error
1	1.646	1.643	-0.22	2.653	2.653	0.00
2	1.823	1.562	-14.31	2.548	2.113	-17.09
3	1.657	1.340	-19.16	1.960	1.590	-18.90
4	1.580	1.643	3.99	2.537	2.723	7.33
5	1.557	1.641	5.37	1.827	1.981	8.44
6	1.911	1.562	-18.30	2.346	1.899	-19.04
7	2.841	2.081	-26.76	2.944	2.231	-24.22
8	4.637	3.642	-21.45	5.369	4.130	-23.07

The other curvatures were normalized using this value, giving the data shown in Table 5.1. The errors shown for the magnitude calibration are much greater than those shown by the shape calibration—the average error for the *y*-scribes is 14.23%. Performing a similar calibration for the *x*-scribes (using the camber for Test Case 9 as the calibration) produces the data shown in Table 5.2 and an average error of 8.51%.

Table 5.2. Full Calibration for *x* scribes (C = 0.06027)

	Crown			Camber		
Test Case	Experimental	Predicted	% error	Experimental	Predicted	% error
9	3.697	3.697	-0.01	1.591	1.591	0.00
10	2.587	2.756	6.52	1.586	1.605	1.26
11	1.821	2.086	14.54	1.242	1.437	15.70
12	1.108	1.314	18.56	0.837	1.036	23.75
15	3.657	3.762	2.85	1.561	1.591	1.94

The substantial errors shown by these full calibrations could have several sources of origin—variation in the AlTiC between rows and variations in scribing parameters such as laser power and instrumentation drift could cause reasonable error. However, the errors do show a general trend—the error appears to be a function of length in both cases. In Table 5.1, the data is calibrated off of Test Case 1 (three 1000μm scribes with 80μm spacing), and the errors for the other 1000μm scribe cases (Test Cases 4 and 5) are reasonable. The 800μm scribe cases (Test Cases 2, 6, 7, and 8) show similar magnitudes of error, and the lone 600μm scribe case shows slightly more error than the 800μm scribe case. A similar trend is exhibited in the *x*-scribes, where test cases 9 through 12 show increasing error with decreasing scribe length. This trend suggests that making the calibration factor C a function of length could greatly improve accuracy.

To find a calibration for the scaling factor as a function of length ($C = C(L)$), the effect of scribe length on curvature was examined for both the finite element analyses and the experimental results. Figure 5.1 is a plot of crown and camber versus scribe length

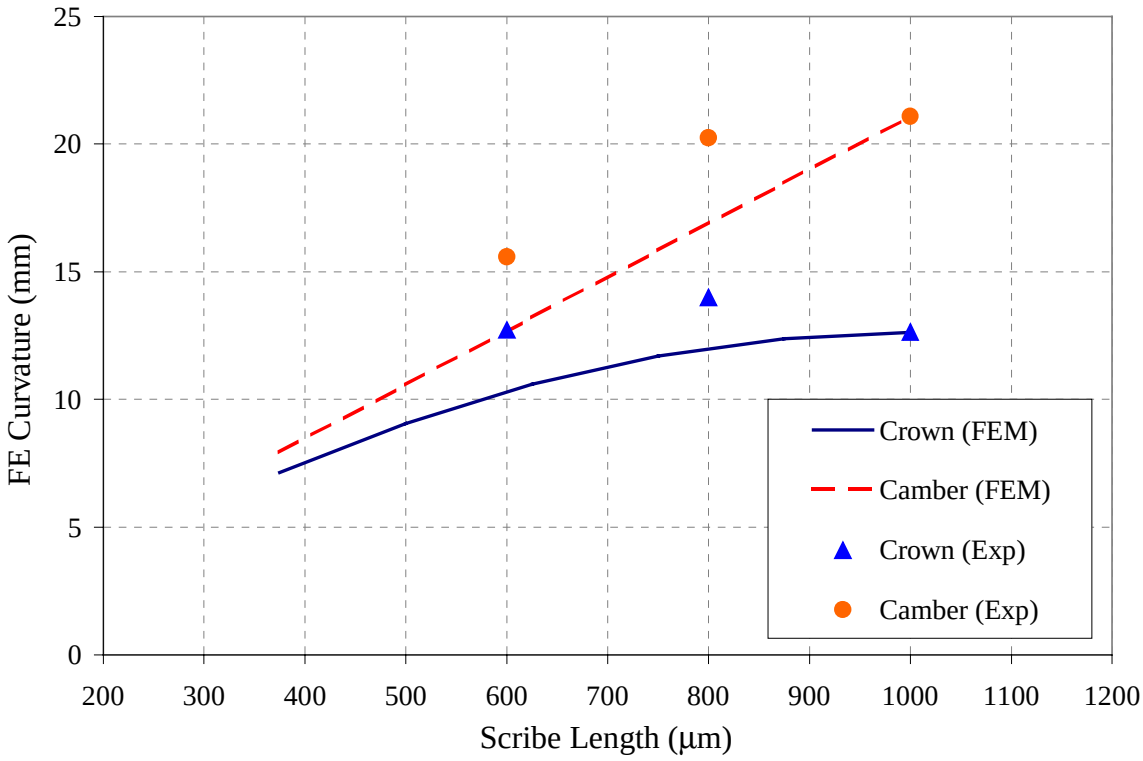

Figure 5.1. Curvature versus Scribe Length for *y*-scribes

for single scribes in the *y*-direction. The finite element method produces two exact curves for the curvatures as functions of length—a parabolic dependence for crown and a linear dependence for camber. These results were obtained by running 12 models for lengths from 375 to 1000μm—the twelve data points exactly fit the curves shown in Figure 5.1. The experimental data points were obtained from Test Cases 1, 2, and 3—the curvatures were normalized such that Test Case 1 exactly matched the predicted values. Figure 5.1 shows that the theoretical model significantly underestimates the curvatures

for scribes shorter than 1000μm, despite producing an accurate crown to camber ratio. Figure 5.2 shows the same plot for scribes in the x direction. The finite element results

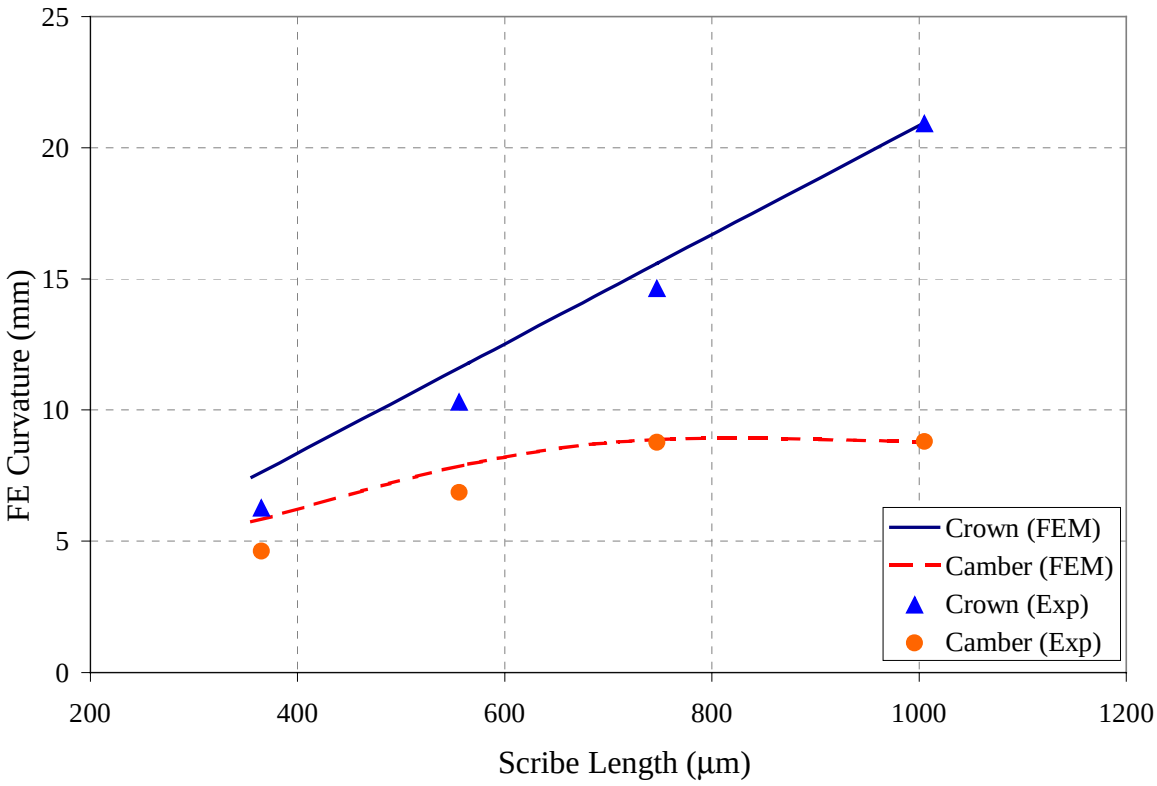

Figure 5.2. Curvature versus Scribe Length for *x*-scribes

show similar trends—the curvature in the direction parallel to the scribe shows quadratic dependence (in this case, camber) and the perpendicular direction has a linear trend (here, crown). The model's predictions for crown and camber are higher than the experimental results, but as with the *y*-scribe cases, the crown to camber ratio is accurate.

Ideally, the curves for the predicted and experimental results would match at every scribe length. A constant scaling factor provides poor results, as shown in Figures 5.1 and 5.2. To increase accuracy, the experimental and predicted curvatures can be calibrated for multiple lengths, giving the scaling factor as a function of length. Figure

5.3 is a plot of scaling factor versus length. Neither the *x* or *y* scribes show a simple

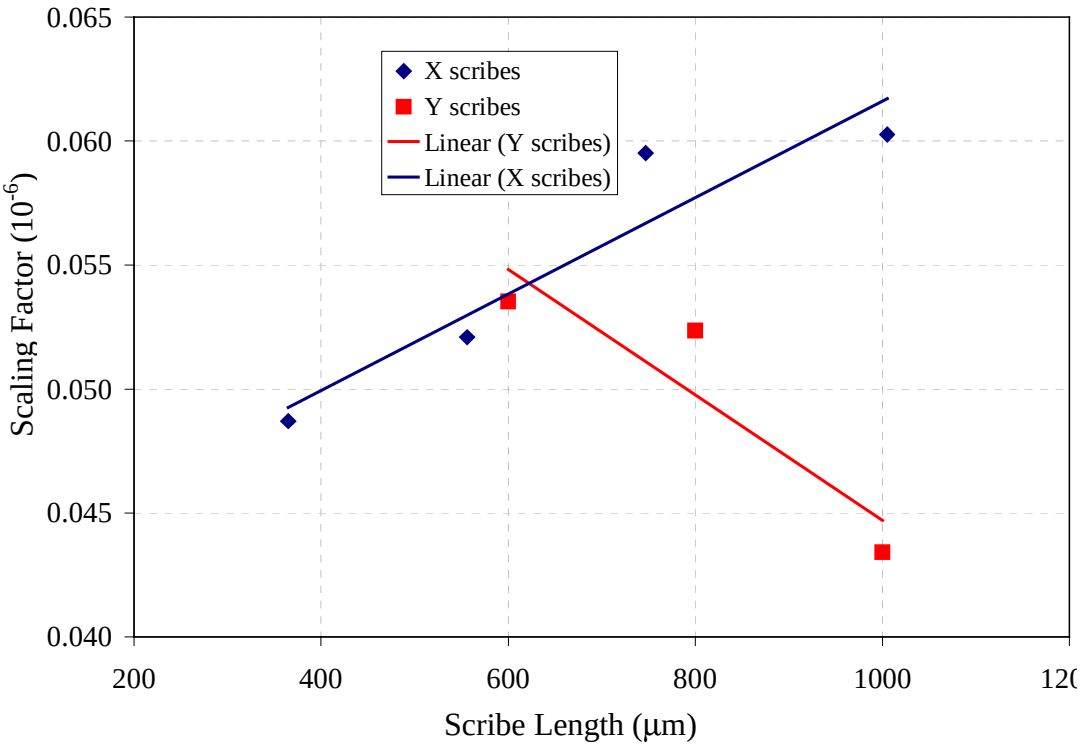

Figure 5.3. Scaling Factor as a Function of Scribe Length

relationship between scribe length and scaling factor, but both show a general trend. The *x* scribes show a general increase in the scaling factor as the scribe length increases; for the *y* scribes, the scaling factor must decrease as scribe length increases for accurate calibration. Further experimentation with more scribe lengths could possibly produce a data set with a more recognizable shape. However, recall that all material and scribing condition variations are lumped into this scaling factor—so, in addition to any actual length dependence, the error caused by inconsistencies in the laser scribing process are shown in the scaling factor. This error can be significant, as shown in Section 5.2.

To simplify the determination of the scaling factor, a linear fit was placed on each of the data sets, producing two equations for the scaling factor as a function of scribe

length. A linear curve was chosen to illustrate the general trend because the lack of data prevents a higher order polynomial or function curve-fit. The two equations are shown below.

$$C_x(L) = (1.95 \times 10^{-5})L + 0.0421 \quad (6)$$

$$C_y(L) = (-2.53 \times 10^{-5})L + 0.070 \quad (7)$$

Using these equations to generate the scaling factors for the test cases, the finite element results were calibrated and compared to the experimental results, resulting in the data shown in Table 5.3. Note the improvement in accuracy over the calibrations shown in

Table 5.3. Calibrated Results Using Scribe Length Dependent Scaling Factor

Test Case	Scaling Factor	Predicted Crown	% error	Predicted Camber	% error
1	0.0447	1.6914	2.74	2.7312	2.96
2	0.0498	1.7919	-1.71	2.4233	-4.89
3	0.0548	1.6911	2.04	2.0064	2.37
4	0.0447	1.6917	7.07	2.8038	10.50
5	0.0447	1.6895	8.49	2.0401	11.65
6	0.0498	1.7912	-6.29	2.1784	-7.13
7	0.0498	2.3870	-15.99	2.5592	-13.08
8	0.0498	4.1781	-9.90	4.7376	-11.75
9	0.0617	3.7845	2.36	1.6286	2.37
10	0.0567	2.5927	0.21	1.5103	-4.74
11	0.0529	1.8305	0.53	1.2611	1.55
12	0.0492	1.0725	-3.22	0.8458	1.01
15	0.0617	3.8507	5.29	1.6290	4.36

Tables 5.1 and 5.2—the average error for all 13 test cases is 5.54%, with a maximum error of 15.99%. This technique for finding the magnitudes of the curvatures could be improved greatly with further experimentation examining the effect of scribe width on the scaling factor.

5.2 **Twist Generation**

All of the previous experimental test cases have utilized scribes that are symmetric with respect to both axes, thus eliminating any asymmetry in the resulting deflection. This asymmetric component, known as twist, is a major manufacturing problem—using laser scribes to eliminate twist while producing the proper crown and camber is one of the major purposes of this study.

To test the ability of the model to predict twist, an asymmetrical scribing pattern was developed. The scribing pattern, shown in Figure 5.4, consists of five scribes in the y-direction—a center 1000μm scribe and four 500μm scribes placed off the centerline to

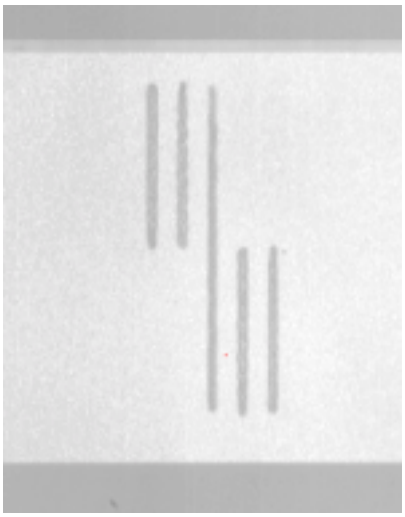

Figure 5.4. Asymmetrical Scribing Pattern

generate twist. The spacing between the scribes is 80μm. In theory, this scribing pattern should generate crown and camber similar to three 1000μm scribes, as well as producing twist (negative twist, using IBM's sign convention).

This scribing pattern was created as a test of the model *after* it had already been calibrated (as shown in Section 5.1). The scribing pattern was placed on 22 sliders at IBM-San Jose (thanks to Hee Park), using the same test procedure described in Section 3.5. The Wyko interferometer was again used to measure the sliders before and after scribing. Great care was taken to ensure the same scribing parameters were used. However, variation in machine setup and the material properties of different batches of AlTiC play a significant role in the curvatures generated by laser scribes. To prevent these factors from influencing the accuracy of the model, the remaining 22 sliders on the row were scribed with test case 1 (three 1000μm scribes in the *y*-direction) to determine if the prior calibration held.

Examining the calibration pattern (the repeat of test case 1) revealed some differences from the original tests. The average crown and camber for the 22 new sliders are 1.8928 nm and 2.8621 nm, respectively, compared to the original values of 1.6464 and 2.6527 nm. Not only were the deflections for the new test greater, but the crown to camber ratio had increased from 0.6207 to 0.6614 (a change of 6.56%). Given that the machine settings were identical, the variation in the AlTiC itself is most likely the source of the differences between the rows. The differing curvatures for the identical scribing pattern illustrates that it is important to consider material effects when modeling and calibrating the scribing pattern.

Initially, the *y*-scribe model with the original F_m = 0.248 N and $C_y(L)$ was used to model the twist-generating pattern. The model was created using the *y*-direction, three slider mesh, and a biquadratic was fit through the data. The crown, camber, and twist were calculated for each of the scribes using equations 3, 4, and 5 in Section 3.2 (note the

factor of four present in the crown and camber definitions, but not the twist). The results were then superposed to give the curvatures for the pattern, shown in Table 5.4. Once

Table 5.4. Experimental and Predicted Results for Twist Test Pattern Using Original Calibration (F_m = 0.248 N)

	Curvature (nm)		
	Experimental	Predicted	% error
Crown	1.9787	2.0105	1.61
Camber	2.8897	3.0574	5.80
Twist	-1.1260	-0.9854	-12.49

again, the model accurately (less than 6% error) predicts the crown and camber generated by the pattern, but the twist error is larger than desired. As mentioned previously, the patterns on this row indicate that a slight change in the calibration could improve the accuracy of the model. Calibrating the model based on the three 1000 μm scribes (Test Case 1) on the same row gives an end force of F_m = 0.260 N. The same scaling factors were used as in Table 5.4. The results for this second calibration are given in Table 5.5.

Table 5.5. Experimental and Predicted Results for Twist Test Pattern Using New Calibration (F_m = 0.260 N)

	Curvature (nm)		
	Experimental	Predicted	% error
Crown	1.9787	2.1324	7.77
Camber	2.8897	3.0358	5.06
Twist	-1.1260	-1.0112	-10.20

The new calibration slightly improves the accuracy of the twist and camber predictions, but the crown prediction is significantly less accurate. However, the new calibration does keep the errors below 10.5%, which is approximately the measurement repeatability of the interferometer for a single slider.

5.3 Parameterization of Scribing Parameters

To solve the inverse problem of determining what scribing pattern produces a desired deflection, the deflection of the scribe must be parameterized. If the scribing system is limited to scribes parallel to the *x* and *y* axes, then the parameterization includes length and center position (*x* and *y* coordinates). For most of the test cases, the scribe is symmetric about the axis perpendicular to the scribe, so only two parameters are needed—length and one coordinate.

For the orthogonal, centered scribes, the finite element models produce linear and quadratic relationships between curvature and scribe length. The lines in Figure 5.1 show the relationship between crown and camber and scribe length for a centered y-direction scribe. However, Figure 5.3 shows that for an accurate calibration, the scaling factor is also a function of length. Using a linear approximation for the scaling factor and the theoretical finite element curves, the crown and camber can be written as functions of scribe length, where the curvatures are in nm when the scribe length is in μm. Figure 5.5

$$Crown_y = (3.42 \times 10^{-10})L^3 - (1.64 \times 10^{-6})L^2 + (1.94 \times 10^{-3})L - 0.0851$$

$$Camber_y = (-5.31 \times 10^{-7})L^2 + (1.47 \times 10^{-3})L + 0.00385$$

shows these curves for the acceptable range of scribe lengths. A similar process can be used to find the empirical curves for the *x*-direction scribes, giving:

$$Crown_x = (4.05 \times 10^{-7})L^2 + (8.77 \times 10^{-4})L + 0.00137$$

$$Camber_x = (2.55 \times 10^{-10})L^3 - (1.14 \times 10^{-7})L^2 + (9.36 \times 10^{-4})L - 0.0259$$

The curvatures generated by the x scribes are plotted in Figure 5.6.

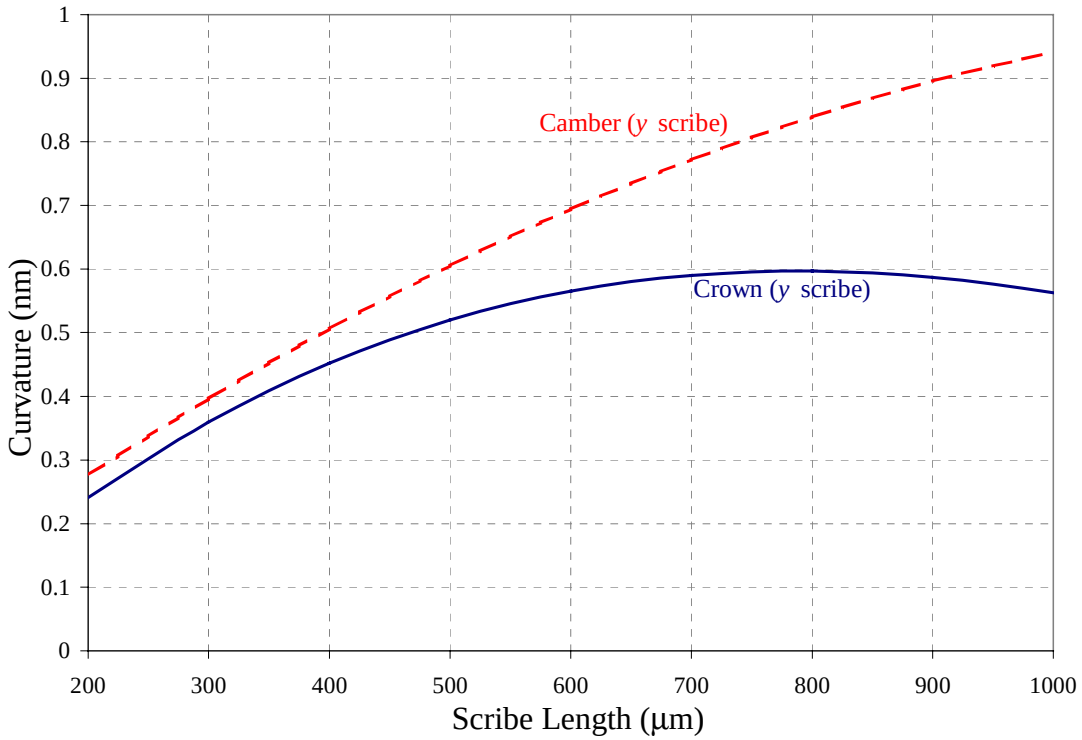

Figure 5.5. Curvature versus Length for Centered *y*-direction Laser Scribes

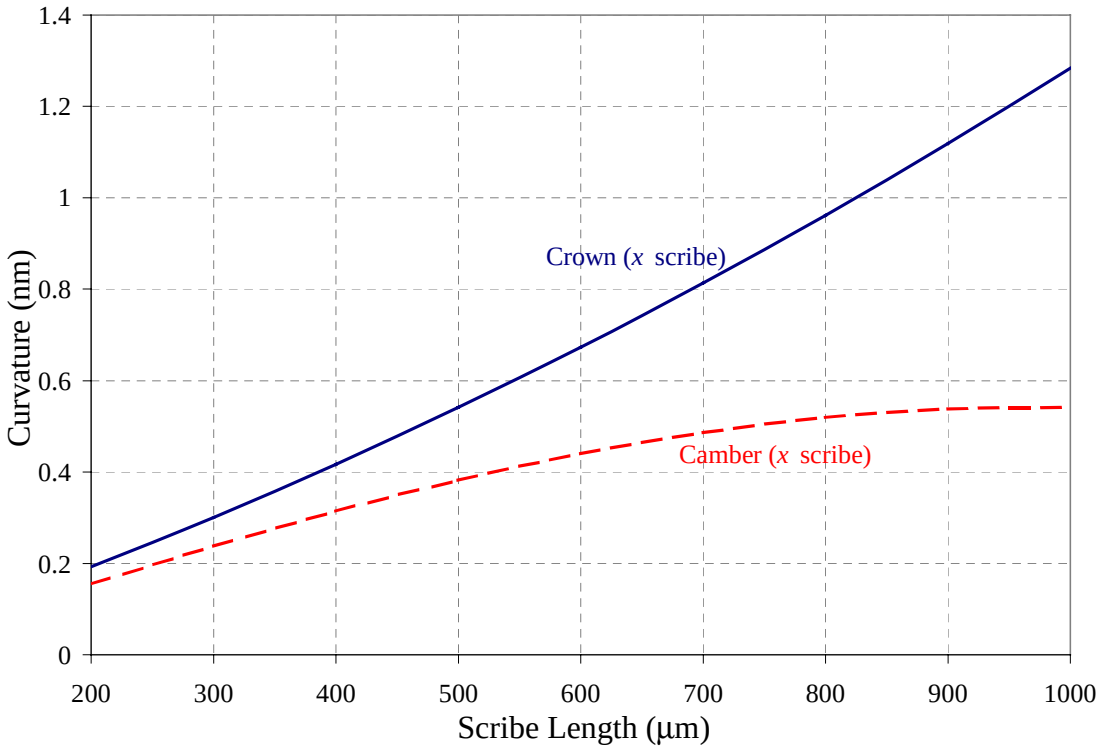

Figure 5.6. Curvature versus Length for Centered *x*-direction Laser Scribe

The position of the center of the scribe is the other parameter used to fully describe the scribing geometry. Defining the center of the slider as $x = 0$ and $y = 0$, establishes a coordinate system for the scribe. Most of the test cases were conducted such that the scribes were placed at the center of the slider and oriented in one direction—i.e. *y* scribes were placed such that $y = 0$ and *x* was varied, while the *x* scribes had $x = 0$ and *y* was varied. This centering technique helped prevent any twist in the resulting data and allowed the parameterization to be carried out with a single coordinate.

Using the shape calibrations found in Section 4.4, three slider finite element models were used to model *x* and *y* direction scribes with varying positions. For the *y*-scribes, the location of the center of the scribe was varied from $x = 0$ (centered on the slider) to $x = 240$ μm. Scribes of length 600, 800 and 1000 micrometers were used at 8 different positions throughout the range. The results for these finite element analyses are shown in Figure 5.7. Note that the vertical axis represents the normalized curvature from the finite element analyses—to find the actual curvature, multiply by the scaling factor for the appropriate length, or mathematically:

$$K_{actual} = C \times K_{FEM}$$

. Both the crown and camber can be accurately expressed ($R^2 > 0.9995$) by a quadratic function of length, although the crown is relatively constant over the entire range. For the *x*-scribes, the position was varied from $y = 0$ to $y = 200$μm. A plot of normalized curvature versus scribe position is shown in Figure 5.8 for scribes of length 556, 747, and 1005μm. The crown and camber are again accurately represented by quadratic functions of scribe position.

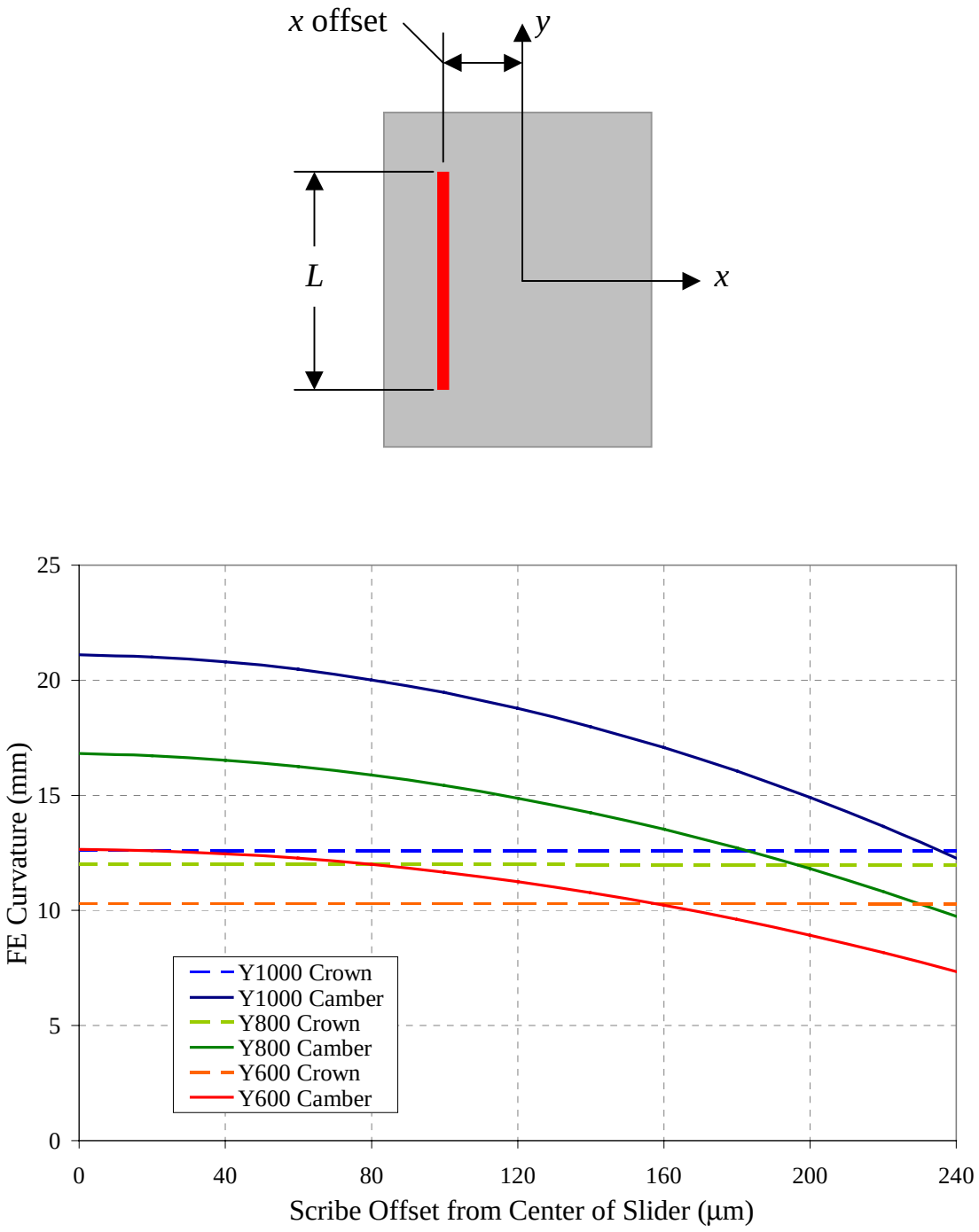

Figure 5.7. Crown and Camber as Functions of Scribe Position for *y*-scribes
Note: Curvatures depicted above are the results of the finite element analyses and must be multiplied by the appropriate scaling factor to give values corresponding to experimental results.

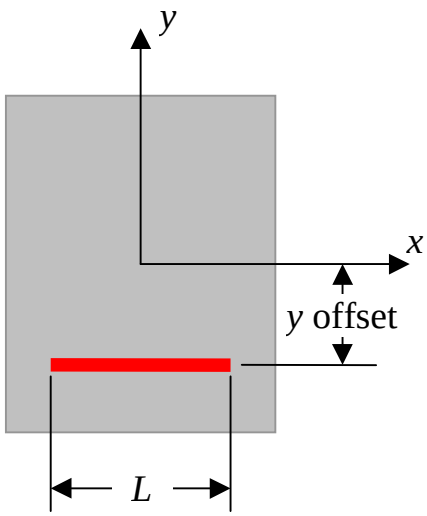

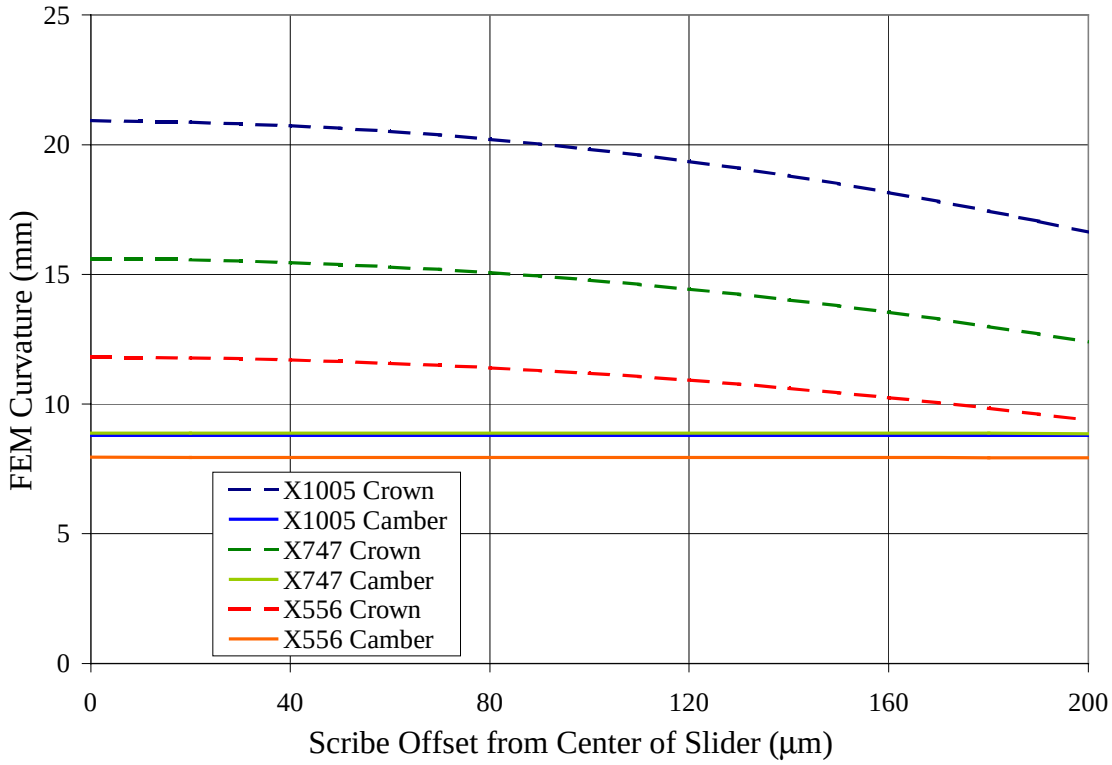

Figure 5.8. Crown and Camber as a Function of Scribe Position for *x*-scribes
Note: Curvatures depicted above are the results of the finite element analyses and must be multiplied by the appropriate scaling factor to give values corresponding to experimental results.

Figures 5.7 and 5.8 allow the computation of the crown and camber for a wide variety of scribing geometries. The normalized crown and camber can be read directly from the graphs for any *x* or *y*-direction scribe centered on the slider in the perpendicular direction.

The actual deflections can be determined by multiplying the normalized curvatures by the scaling factor for the appropriate length (determined from equations 6 and 7 given in Section 5.1). Calibration data suggests that the results should exhibit less than 5% error.

5.4 Summary

The ability of the calibrated end-force model to predict curvatures generated by laser scribes has been demonstrated. The solutions rely on linear finite element models. The scaling factors for curvature are dependent on scribe length, as shown in Figure 5.3 and equations 6 and 7. Using the experimentally calibrated models, the predicted curvatures for 13 experimental scribing patterns yielded less than 6% error over the entire range. A further test of asymmetric scribes yielded less than 6% error for crown and camber and 12.5% error for twist.

x-direction calibration	*y*-direction calibration
f_M = 10 N/mm	f_M = 10 N/mm
F_m = 0.213 N	F_m = 0.248 N
$C_x(L) = (1.95 \times 10^{-5})L + 0.042$	$C_y(L) = (-2.53 \times 10^{-5})L + 0.070$

The results of the analysis of the laser scribing process have some important implications. The model itself (the end forces and line dipole) produces very accurate crown to camber ratios for the appropriate ratio of F_m to f_M. However, two distinctly different calibrations are needed for scribes—scribes in the y direction require a 16% greater end force, and using the improper calibration results in errors exceeding 20%. This directional dependence could have several sources: anisotropic properties of the AlTiC, actual differences in the scribing process along the different axes, or a different residual stress state before scribing. The variation in the scaling factor with length suggests there is unknown physics in the laser scribing process. This variation could be due to some interaction with the residual stress in the row prior to scribing or some directional dependence of the scribe itself. Furthermore, the dependence on length is directionally dependent—another indication of anisotropic properties in either the material or the residual stress state. Also, the two different sets of experiments note that different batches of material can produce minor variations in results

Despite these considerations, however, the calibrated model does offer good accuracy (even for the twist generating case), the error often being smaller than the measurement repeatability of the interferometer.

6 Conclusions and Recommendations

6.1 Conclusions

1. Experimentally calibrated line-force dipole systems were developed that accurately model the deflections produced by mechanical and laser scribing on flat plates.
2. Finite element techniques were developed to allow modeling of complicated and multiple scribe geometries. The techniques can be easily extended to other plate and scribing geometries for future changes in manufacturing.
3. Experimental calibration revealed material and scribe-length dependence on the deflections created by laser scribing. Parameterization of these factors allowed for improved accuracy.
4. The models were parameterized for direction and scribe placement, thus allowing the determination of the deflections produced by an arbitrary scribe with a high degree of accuracy.
5. The accuracy and flexibility of the model was tested using an asymmetrical scribe pattern, and the model yielded accurate results despite varied conditions.

6.2 Recommendations for Further Research

1. The present research calibrated the line-dipole models from experimental results on a single batch of material (AlTiC). Preliminary trials with other batches of AlTiC have revealed some material dependence that should be explored.

2. The mechanical and laser scribing techniques should work for any brittle material or possibly even metals. Experimentation with other materials could reveal additional uses for the technique.
3. The physical principles of laser scribing (e.g. influence of laser power, scribe interaction with residual stress in the material, actual mechanism for inducing stress) are not well understood. Further general exploration into this area would be beneficial in understanding the technique.

References

Ahn, Y., T. N. Farris, and S. Chandraskar, “Elastic Stress Fields Caused by Sliding Microindentation of Brittle Materials,” Proceedings of the International Conference On Machining of Advanced Materials, S. Jahanimir, ed., NIST Special Publication 847, 1993.

Austin, Brad, Masters Thesis, North Carolina State University, 2000.

Liu, D. M., et. al., “Laser-induced Deformation on a Hard Disk Surface,” Applied Surface Science, volume 138-139, 482-488, 1999.

Tam, A.C., C.C. Poon, L. Crawforth, and P. M. Lundquist, “Manufacturing: Stress on the Dotted Line,” IBM Publications, Almaden Research Center, Volume 6, Issue 13, December 1999.

Yoffe, E. H., “Elastic Stress Fields Caused by Indenting Brittle Materials,” Phil. Mag. A, Vol. 46, No. 4, 1982.

A Raw Data from Experimental Tests

The following five pages contain the experimental data for the laser scribing tests conducted at IBM-San Jose. The procedure by which data was collected is outlined in Section 3.3. All measurements were conducted using a Wyko HD-2000 laser interferometer (which relies on light phase shift to determine the height), and IBM's internal Advanced Air Bearing Analysis program was used to compute the curvatures. The average instrument repeatability was found to be ±0.15 nm, and the standard deviations of the repeated scribing patterns reflect this repeatability.

Note that certain sliders on certain rows were deleted from the test. Most of the sliders removed from the data set were sliders on the ends of rows that gave erroneous results due to inconsistent boundary conditions. Sliders 12 through 22 on Row 5 were deleted because of drift in the LCAT machine itself that resulted in inconsistent scribe spacing. Furthermore, note that the data shown in the tables is the curvature after scribing minus the curvature before scribing—the absolute magnitudes were removed for confidentiality purposes.

IBM Laser Scribing Experimental Results: Row 1.

Slider No	Crown	Camber	Twist
1	1.94	1.86	1.20
2	2.31	2.01	0.15
3	1.78	1.79	0.27
4	1.82	1.73	0.11
5	1.65	1.74	0.11
6	1.66	1.75	-0.06
7	1.74	1.74	0.19
8	1.74	1.86	0.36
9	1.37	1.94	0.01
10	1.00	1.84	1.80
11	2.05	1.84	-0.16
12	2.28	1.86	-0.24
13	1.90	1.82	-0.12
14	1.68	1.80	0.03
15	2.27	1.84	0.05
16	1.84	1.73	-0.07
17	1.35	1.73	0.28
18	1.74	1.78	-0.09
19	1.52	1.81	0.26
20	2.03	1.71	-0.06
21	1.59	1.68	-0.20
22	2.02	1.76	0.12
23	1.87	1.69	0.09
24	1.64	1.94	0.21
25	2.00	1.72	-0.33
26	1.62	1.66	-0.11
27	2.08	1.74	0.12
28	1.46	1.63	0.29
29	1.64	1.68	0.02
30	1.75	1.71	-0.44
31	1.65	1.59	0.06
32	1.68	1.80	-0.33
33	1.53	1.57	-0.29
34	2.03	1.80	-0.12
35	1.67	1.54	0.12

Slider No	Crown	Camber	Twist
36	1.92	1.69	0.02
37	1.55	1.68	0.13
38	2.30	1.77	-0.03
39	1.97	1.72	-0.22
40	1.35	1.53	0.08
41	1.35	1.44	-0.44
42	1.81	1.52	0.25
43	1.64	1.47	0.28
44	1.08	1.25	-0.39

Scribing Patterns

Sliders 1-44: 3 *x* scribes
Length: 1005 μm
Spacing: 400 μm
Avg. Crown: 1.75 nm
Avg. Camber: 1.72 nm
Avg. Twist: 0.07 nm

IBM Laser Scribing Experimental Results: Row 2.

Slider No	Crown	Camber	Twist
1	2.38	1.60	0.91
2	3.04	1.66	0.18
3	2.97	1.66	0.05
4	2.85	1.59	1.71
5	3.16	1.71	0.02
6	3.02	1.74	-0.51
7	3.24	1.69	-0.22
8	3.15	1.72	-0.12
9	3.37	1.77	-0.26
10	3.50	1.78	-0.47
11	3.14	1.67	-0.27
12	3.22	1.32	-0.38
13	3.52	1.51	-0.29
14	3.66	1.59	-0.37
15	3.67	1.65	0.21
16	3.81	1.67	-0.45
17	3.74	1.64	0.17
18	3.89	1.63	-0.32
19	3.59	1.56	0.31
20	3.80	1.63	-0.51
21	3.99	1.65	-1.03
22	3.67	1.65	-0.31
23	3.23	1.37	-0.50
24	3.38	1.43	-0.50
25	3.52	1.50	-0.62
26	3.75	1.54	-0.67
27	3.70	1.84	-1.39
28	3.58	1.58	-0.14
29	3.83	1.61	-0.77
30	3.87	1.57	-0.85
31	3.71	1.61	0.06
32	3.77	1.57	-0.41
33	3.89	1.55	0.17
34	4.24	3.52	-0.30

Slider No	Crown	Camber	Twist
36	4.25	3.28	-0.83
37	4.53	3.48	-0.46
38	4.50	3.32	-0.51
39	4.22	3.34	-0.13
40	4.42	3.37	-0.90
41	4.16	3.18	-0.35
42	3.99	2.95	-0.43
43	3.78	2.82	-0.41
44	3.32	2.81	-0.95

Scribing Patterns

Sliders 1-11: 3 *x* scribes
Length: 1005 μm Spacing: 200 μm
Avg. Crown: 3.07 nm
Avg. Camber: 1.69 nm
Avg. Twist: -0.03 nm

Sliders 12-22: 3 *x* scribes
Length: 1005 μm Spacing: 80 μm
Avg. Crown: 3.69 nm
Avg. Camber: 1.59 nm
Avg. Twist: -0.27 nm

Sliders 23-33: 3 *x* scribes
Length: 1005 μm Spacing: 40 μm
Avg. Crown: 3.66 nm
Avg. Camber: 1.56 nm
Avg. Twist: -0.51 nm

Sliders 34-44: 5 *x* scribes
Length: 1005 μm Spacing: 200 μm
Avg. Crown: 4.17 nm
Avg. Camber: 3.23 nm
Avg. Twist: -0.44 nm

IBM Laser Scribing Experimental Results: Row 3.

Slider No	Crown	Camber	Twist
1	2.12	1.51	0.79
2	2.66	1.57	0.38
3	2.40	1.44	0.56
4	2.81	1.68	0.03
5	2.40	1.48	0.01
6	2.58	1.60	0.03
7	2.68	1.65	-0.13
8	2.60	1.57	0.11
9	2.78	1.68	0.28
10	2.81	1.64	0.02
11	2.62	1.62	-0.14
12	1.96	1.14	-0.39
13	1.81	1.21	-0.01
14	1.96	1.22	0.23
15	1.71	1.29	0.07
16	1.94	1.30	-0.04
17	1.82	1.25	-0.15
18	1.79	1.22	0.02
19	1.82	1.18	0.01
20	2.04	1.27	0.09
21	1.60	1.26	0.24
22	1.58	1.32	-0.21
23	1.10	0.77	-0.35
24	1.21	0.83	-0.09
25	1.20	0.83	-0.14
26	1.11	0.83	0.05
27	1.06	0.83	-0.20
28	1.03	0.84	-0.05
29	1.09	0.87	0.06
30	1.07	0.82	-0.28
31	1.05	0.86	-0.09
32	1.06	0.84	-0.10
33	1.21	0.89	-0.01

Scribing Patterns

Sliders 1-11: 3 *x* scribes
Length: 747 μm Spacing: 80 μm
Avg. Crown: 2.59 nm
Avg. Camber: 1.59 nm
Avg. Twist: 0.17 nm

Sliders 12-22: 3 *x* scribes
Length: 556 μm Spacing: 80 μm
Avg. Crown: 1.82 nm
Avg. Camber: 1.24 nm
Avg. Twist: -0.01 nm

Sliders 23-33: 3 *x* scribes
Length: 365 μm Spacing: 80 μm
Avg. Crown: 1.11 nm
Avg. Camber: 0.84 nm
Avg. Twist: -0.11 nm

IBM Laser Scribing Experimental Results: Row 4.

Slider No	Crown	Camber	Twist
4	2.03	3.15	-0.56
5	1.61	2.55	-0.12
6	1.54	2.57	0.09
7	1.35	2.49	-0.16
8	1.65	2.61	0.16
9	1.53	2.56	-0.09
10	1.71	2.69	0.09
11	1.72	2.62	0.00
12	1.55	2.58	-0.01
13	1.64	2.67	0.13
14	1.78	2.69	-0.08
15	1.32	2.39	-0.33
16	1.62	2.49	-0.17
17	1.70	2.61	0.38
18	1.57	2.53	0.35
19	1.65	2.52	0.01
20	1.43	2.53	-0.14
21	1.54	2.47	-0.17
22	1.58	2.43	0.20
23	1.58	1.79	0.17
24	1.59	1.83	0.12
25	1.42	1.89	-0.26
26	1.58	1.81	-0.17
27	1.70	1.87	0.06
28	1.52	1.86	-0.21
29	1.69	1.88	0.34
30	1.48	1.79	-0.01
31	1.50	1.81	-0.17
32	1.50	1.77	-0.17
33	1.57	1.80	-0.08
34	1.73	1.93	0.18
35	1.87	2.09	-0.05
36	1.71	2.01	-0.05
37	1.51	1.93	-0.39
38	1.71	1.92	-0.38
39	1.55	1.89	-0.25
40	1.69	2.01	-0.38
41	1.66	1.99	-0.21
42	1.49	1.78	-0.32
43	1.70	2.00	-0.23
44	1.61	2.01	-0.26

Scribing Patterns

Sliders 4-14: 3 *y* scribes
Length: 1000 μm Spacing: 80 μm
Avg. Crown: 1.65 nm
Avg. Camber: 2.65 nm
Avg. Twist: -0.05 nm

Sliders 15-22: 3 *y* scribes
Length: 1000 μm Spacing: 40 μm
Avg. Crown: 1.58 nm
Avg. Camber: 2.54 nm
Avg. Twist: 0.02 nm

Sliders 23-33: 3 *y* scribes
Length: 1000 μm Spacing: 240 μm
Avg. Crown: 1.56 nm
Avg. Camber: 1.83 nm
Avg. Twist: -0.03 nm

Sliders 34-44: 3 *y* scribes
Length: 600 μm Spacing: 80 μm
Avg. Crown: 1.66 nm
Avg. Camber: 1.96 nm
Avg. Twist: -0.21 nm

IBM Laser Scribing Experimental Results: Row 5.

Slider No	Crown	Camber	Twist
2	1.59	2.43	0.13
3	2.05	2.70	0.06
4	1.79	2.49	0.01
5	1.64	2.39	0.05
6	1.77	2.48	0.02
7	1.90	2.56	0.08
8	2.02	2.61	0.05
9	2.05	2.61	0.15
10	1.65	2.56	0.12
11	1.77	2.65	0.24
23	1.89	2.23	0.03
24	1.85	2.36	0.11
25	1.81	2.31	0.29
26	1.92	2.40	-0.06
27	1.99	2.39	-0.22
28	1.86	2.32	0.01
29	2.06	2.41	0.24
30	2.48	2.66	0.32
31	2.68	2.89	-0.34
32	2.90	3.01	-0.42
33	2.84	3.01	-0.39
34	3.22	3.03	-0.41
35	2.70	3.00	-0.08
36	3.07	3.01	0.26
37	4.15	4.86	-0.11
38	4.56	5.16	-0.23
39	4.93	5.45	-0.58
40	4.92	5.53	-0.74
41	4.89	5.39	-0.61
42	4.89	5.51	-0.36
43	4.12	5.68	-1.09

Scribing Patterns

Sliders 2-11: 3 *y* scribes
Length: 800 µm Spacing: 80 µm
Avg. Crown: 1.82 nm
Avg. Camber: 2.55 nm
Avg. Twist: 0.09 nm

Sliders 23-29: 3 *y* scribes
Length: 800 µm Spacing: 160 µm
Avg. Crown: 1.91 nm
Avg. Camber: 2.35 nm
Avg. Twist: 0.06 nm

Sliders 30-36: 4 *y* scribes
Length: 800 µm Spacing: 160 µm
Avg. Crown: 2.84 nm
Avg. Camber: 2.94 nm
Avg. Twist: -0.15 nm

Sliders 37-43: 7 *y* scribes
Length: 800 µm Spacing: 80 µm
Avg. Crown: 4.64 nm
Avg. Camber: 5.37 nm
Avg. Twist: -0.53 nm

B Finite Element Models

To model all of the scribing situations, several models were necessary to encompass the wide range of scribe lengths and geometries. The models were made as modular as possible to prevent a totally new model from being generated for each scribe geometry. Sections 4.3 and 4.4 give general overviews of the results and modeling techniques. The following five pages give the specific details for the finite element analyses (which were conducted using ANSYS 5.6).

Single Slider Model – x scribes

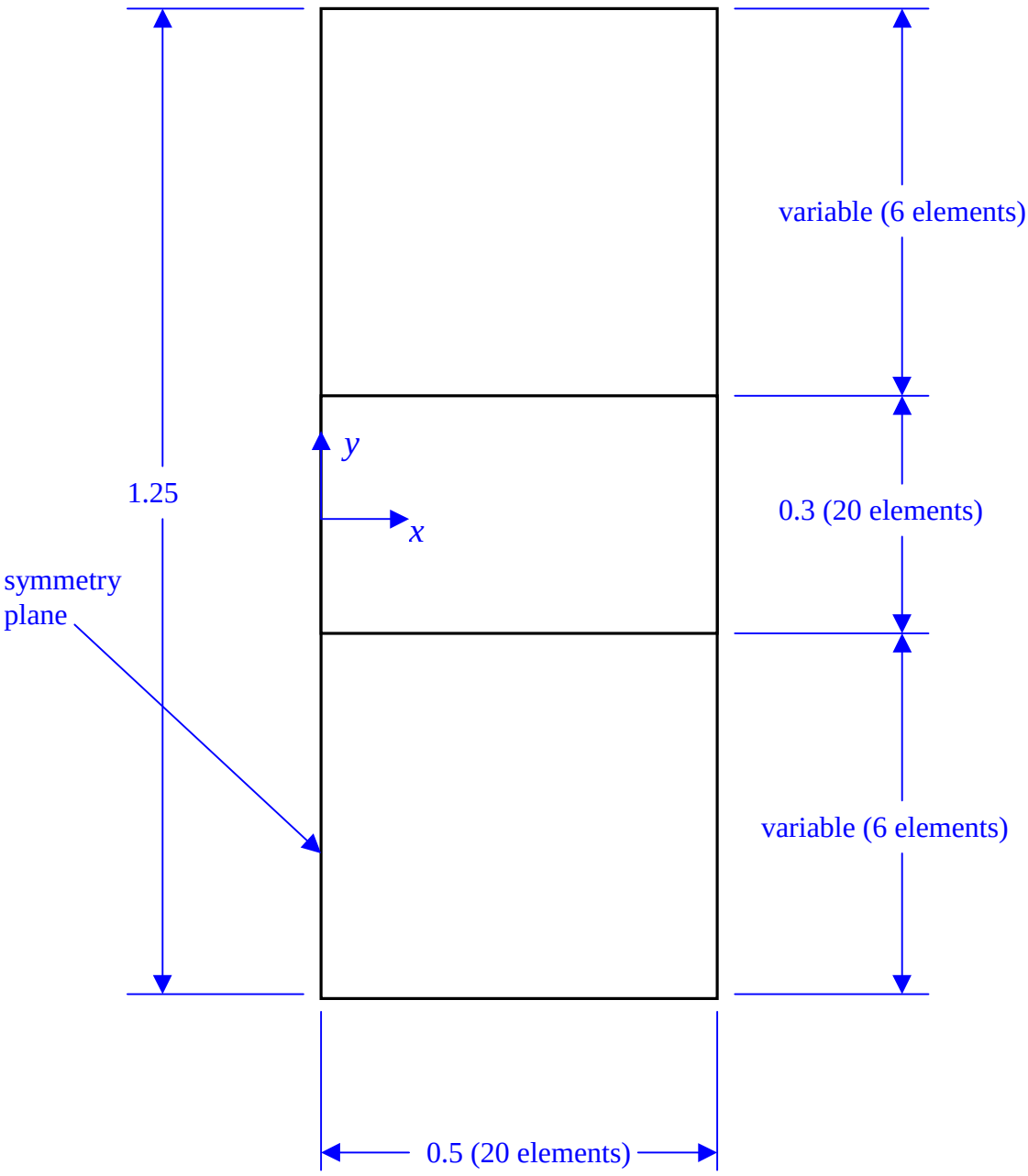

Note: Model has 10 elements with a geometric gradient of 5 (the tenth element is five times longer than the first) through the thickness of 0.3.

Single Slider Model – y scribes

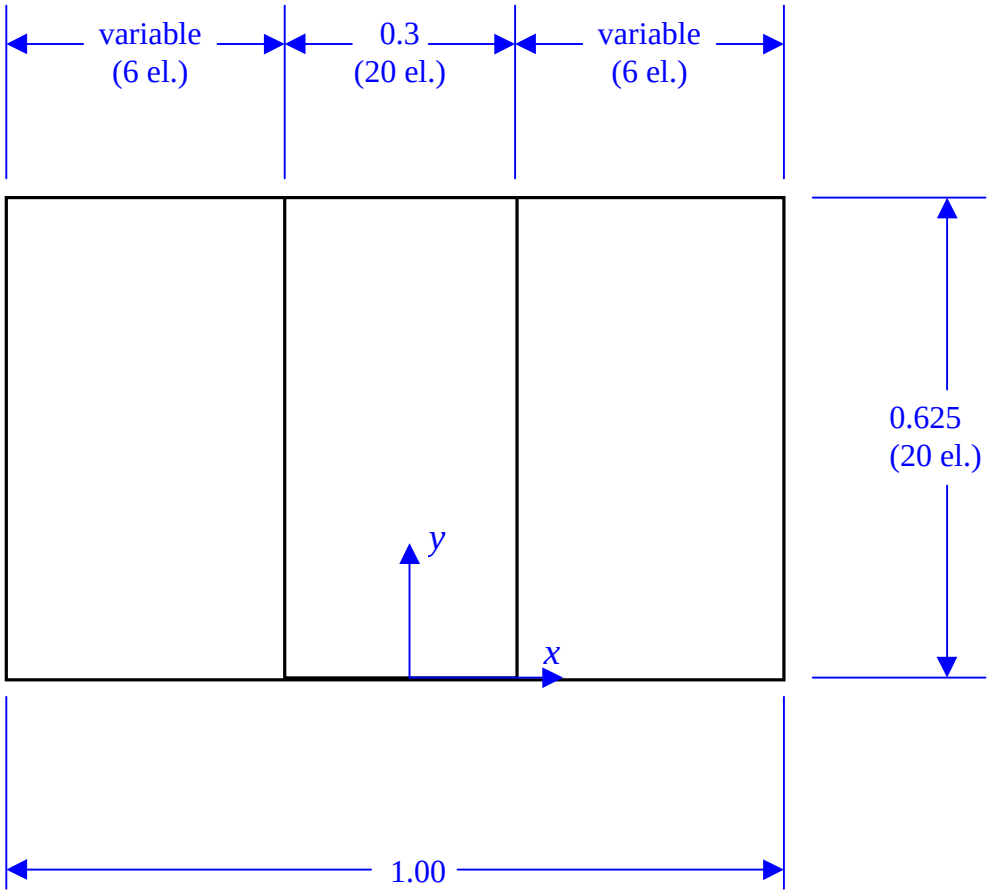

Note: Model has 10 elements with a geometric gradient of 5 (the tenth element is five times longer than the first) through the thickness of 0.3.

Three Slider Model – x scribes

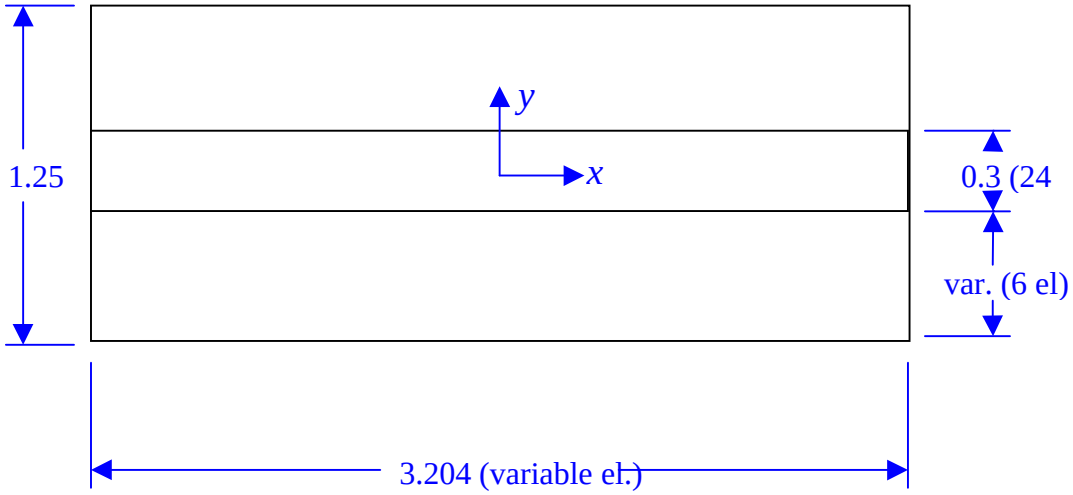

Note: Model has 10 elements with a geometric gradient of 5 (the tenth element is five times longer than the first) through the thickness of 0.3.

The variation in elements along the *x*-axis depends on the scribe length. The number of elements was adjusted to allow a fairly accurate representation of the experimental scribe length. Shown below in the table is the number of elements used along the *x*-axis depending on scribe length.

Experimental Scribe Length	No. divisions on x axis	No. divisions per scribe	Modeled Scribe Length
365 µm	45	5	356 µm
556 µm	51	9	565 µm
747 µm	20	14	748 µm

Three Slider Model – y scribes

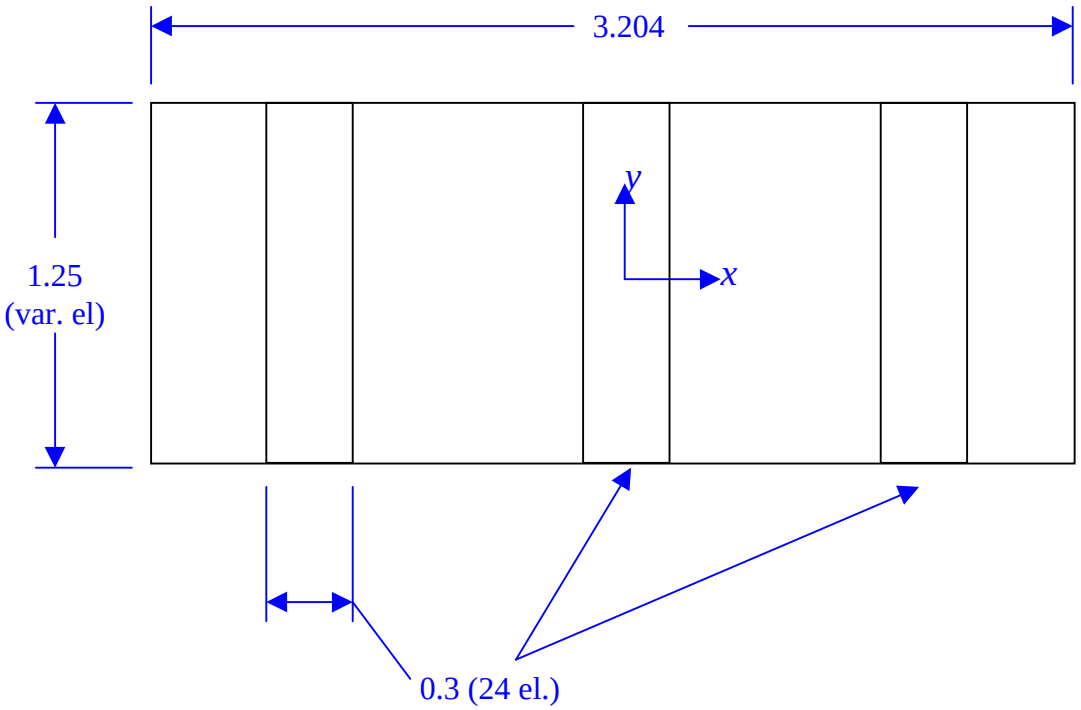

Note: Model has 10 elements with a geometric gradient of 5 (the tenth element is five times longer than the first) through the thickness of 0.3.

The variation in elements along the *y*-axis depends on the scribe length. The number of elements was adjusted to allow a fairly accurate representation of the experimental scribe length. Shown below in the table is the number of elements used along the *y*-axis depending on scribe length.

Experimental Scribe Length	No. divisions on y axis	No. divisions per scribe	Modeled Scribe Length
600 µm	23	11	598 µm
800 µm	22	14	796 µm
1000 µm	20	16	1000 µm

Three Slider Model – x scribes (L = 1005 μm)

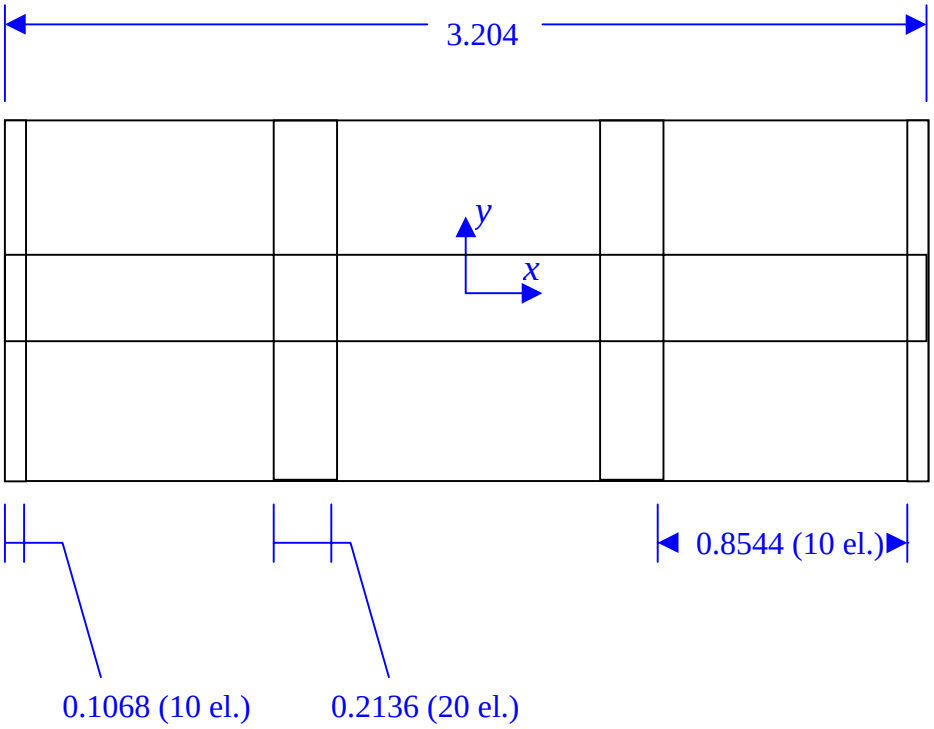

The three-slider model for 1005 μm *x*-scribes incorporates a densely meshed region around the scribe tips (the spacing is uniform—the three sliders are identical). Otherwise, it is identical to the three-slider model for standard *x*-scribes (the element numbers and dimensions in the *y* direction are identical).

C Calibrating Finite Element Models

The force system used to model laser scribes requires that calibration to match experimentally determined results. The calibration technique, as discussed in section 4.2, calibrates the shape of slider (the crown to camber ratio) by varying the ratio of f_M to F_m. The final magnitude of curvature is found by scaling the curvatures with a scaling factor (shown in section 5.1 to exhibit a dependence on length).

Since the ratio of f_M to F_m is the important quantity, f_M was held fixed, and F_m was varied. For the single slider models, a calibration factor was found by simply running finite element analyses of a specified geometry until one of the values of F_m yielded a crown to camber ratio that matched the experimental value (results are shown in section 4.3). However, during this analysis, it was observed that for any given geometry, crown and camber vary linearly with F_m, thus allowing the crown and camber for an arbitrary F_m to be interpolated from the curvatures of two known values of F_m. This principle also held when it was tested with the three-slider models.

To use this technique to aid in calibration, two sets of data was taken for every necessary model (F_m = 0.23 N and F_m = 0.25 N to correspond with f_M = 10 N/mm). The data was placed in a spreadsheet with the interpolation formulas; using the spreadsheet, F_m could be varied to change the calibration without running additional finite element analyses. The scaling factor C was also incorporated into the spreadsheet for determination of the actual magnitudes of the curvatures. The tables on the following two pages contain the finite element output for the two values of F_m—the actual results shown in Chapters 4 and 5 can be linearly interpolated from this data.

Calibration Data for Three Slider Model

F_m = 0.23 N

Direction	Length (μm)	Location (μm from center)	Crown (FEM)	Camber (FEM)
y	1000	0	11.524	21.306
y	1000	40	11.522	21.028
y	1000	80	11.520	20.214
y	1000	200	11.500	12.458
y	800	0	10.988	16.958
y	800	80	10.984	16.087
y	800	160	10.977	13.623
y	800	240	10.966	9.909
y	600	0	9.440	12.754
y	600	80	9.436	12.099
x	1005	0	20.764	9.689
x	1005	40	20.583	9.689
x	1005	80	20.047	9.688
x	1005	200	16.465	9.688
x	1005	400	6.026	9.684
x	747	0	15.479	9.727
x	747	80	14.944	9.725
x	556	0	11.713	8.685
x	556	80	11.309	8.682
x	365	0	7.379	6.254
x	365	80	7.124	6.251

Notes

1) All curvature data is in finite element units and can be scaled linearly to find actual curvatures using the scaling factor (see Section 5.1).
2) The data above represents f_M = 10 N/mm and F_m = 0.23 N. Linear interpolation is valid only when F_m is varied without varying f_M.

Calibration Data for Three Slider Model

$F_m = 0.25$

Direction	Length (μm)	Location (μm from center)	Crown (FEM)	Camber (FEM)
y	1000	0	12.743	21.068
y	1000	40	12.740	20.792
y	1000	80	12.738	19.980
y	1000	200	12.716	12.252
y	800	0	12.113	16.781
y	800	80	12.109	15.913
y	800	160	12.101	13.454
y	800	240	12.089	9.747
y	600	0	10.387	12.628
y	600	80	10.383	11.974
x	1005	0	20.574	10.748
x	1005	40	20.391	10.748
x	1005	80	19.856	10.749
x	1005	200	16.270	10.748
x	1005	400	5.823	10.748
x	747	0	15.336	10.735
x	747	80	14.801	10.733
x	556	0	11.605	9.563
x	556	80	11.200	9.560
x	365	0	7.310	6.875
x	365	80	7.055	6.872

Notes

1) All curvature data is in finite element units and can be scaled linearly to find actual curvatures using the scaling factor (see Section 5.1).
2) The data above represents f_M = 10 N/mm and F_m = 0.25 N. Linear interpolation is valid only when F_m is varied without varying f_M.